Stem Cell Reports
Article

ISSCR

OPEN ACCESS

DIDO as a Switchboard that Regulates Self-Renewal and Differentiation in Embryonic Stem Cells

Agnes Fütterer,[1] Jésus de Celis,[1] Rosana Navajas,[2] Luis Almonacid,[3] Julio Gutiérrez,[1] Amaia Talavera-Gutiérrez,[1] Cristina Pacios-Bras,[1] Ilenia Bernascone,[4] Fernando Martin-Belmonte,[4] and Carlos Martinéz-A[1,*]

[1]Department of Immunology and Oncology
[2]Proteomics Unit, ProteoRed ISCIII
[3]Genomics Unit, Q-PCR Facility
Centro Nacional de Biotecnología (CNB-CSIC), Darwin 3, 28049 Madrid, Spain
[4]Department of Development and Differentiation, Centro de Biología Molecular Severo Ochoa, CSIC-Universidad Autónoma de Madrid, 28049 Madrid, Spain
*Correspondence: cmartineza@cnb.csic.es
http://dx.doi.org/10.1016/j.stemcr.2017.02.013

SUMMARY

Transition from symmetric to asymmetric cell division requires precise coordination of differential gene expression. We show that embryonic stem cells (ESCs) mainly express DIDO3 and that their differentiation after leukemia inhibitory factor withdrawal requires DIDO1 expression. C-terminal truncation of DIDO3 (*Dido3ΔCT*) impedes ESC differentiation while retaining self-renewal; small hairpin RNA-*Dido1* ESCs have the same phenotype. *Dido3ΔCT* ESC differentiation is rescued by ectopic expression of DIDO3, which binds the *Dido* locus via H3K4me3 and RNA POL II and induces DIDO1 expression. DIDO1, which is exported to cytoplasm, associates with, and is N-terminally phosphorylated by PKCiota. It binds the E3 ubiquitin ligase WWP2, which contributes to cell fate by OCT4 degradation, to allow expression of primitive endoderm (PE) markers. PE formation also depends on phosphorylated DIDO3 localization to centrosomes, which ensures their correct positioning for PE cell polarization. We propose that DIDO isoforms act as a switchboard that regulates genetic programs for ESC transition from pluripotency maintenance to promotion of differentiation.

INTRODUCTION

Mouse embryonic stem cells (ESCs) from early-stage embryos have indefinite self-renewal capacity and can differentiate into cell types derivative of all three germ layers through asymmetric cell division (Niwa, 2007). Asymmetric cell division is a complex process whereby transcription, cell differentiation, cell cycle, and cell polarity must be coordinated in time and space (Noatynska et al., 2013). In vitro embryoid bodies (EBs) are powerful tools with which to study and understand the molecular mechanisms that underlie this process, as they mimic the in vivo developmental stages of peri-implantation embryos from epiblast to egg cylinder stages. An early step in this process is formation of the primitive endoderm (PE), an outer layer of polarized cells, followed by epiblast and primitive ectoderm development (Niwa, 2010).

Genome-wide screens have identified many potential regulators of stem cell function. These include genes with established roles in transcription regulation, cell growth, and differentiation, as well as genes whose function is largely unknown or remains to be validated in the context of stem cell biology, including the *Dido* (death inducer obliterator) gene (Kim et al., 2008; Kidder et al., 2008; Chen et al., 2008; Brandenberger et al., 2004).

We identified *Dido*, a complex gene that encodes three proteins generated by alternative splicing. From smallest to largest, these isoforms are DIDO1, DIDO2, and DIDO3; they have a common N-terminal region and isoform-specific C-terminal parts (Futterer et al., 2005). DIDO3 composition, as determined by bioinformatics analysis, suggests that it helps maintain genomic stability (Rojas et al., 2005). DIDO3 comprises a plant homeodomain (PHD) finger, a transcription elongation factor S-II subunit M (TFSIIM) domain, a Spen paralog and ortholog (SPOC) module, and a long C-terminal region (CT) of unknown homology (Rojas et al., 2005; Futterer et al., 2005). The exact functions of DIDO3 TFSIIM and SPOC modules have not yet been defined. In the TFIIS transcription elongation factor, the TFSIIM domain binds to and facilitates RNA polymerase II activity (Kettenberger et al., 2003); the SPOC module is linked to Spen family proteins, which are involved in transcriptional repression (Sanchez-Pulido et al., 2004). The PHD, one of a large group of zinc-finger proteins, recognizes post-translationally modified histone tails, including methylated lysine residues (Musselman and Kutateladze, 2011).

We determined the crystal structure of the DIDO PHD finger in complex with histone 3 trimethylated on lysine 4 (H3K4me3), which showed an atypical aromatic cage-like binding site bearing a histidine residue. Biochemical, structural, and mutational analyses of this complex identified specificity and affinity determinants for DIDO PHD binding, which is disrupted by threonine

3 phosphorylation and triggers DIDO3 translocation from chromatin (Gatchalian et al., 2013).

DIDO1 localizes in the nucleus and cytosol, whereas DIDO2 is found only in the nucleus (Futterer et al., 2005). DIDO3, located primarily in the nucleus and centrosomes (Trachana et al., 2007), is expressed strongly in ESCs and decreases during development; expression is weaker in somatic cells, but recovers in induced pluripotent stem cells generated from somatic cells (Gatchalian et al., 2013).

All attempts to date to delete DIDO in cell lines or in mice show that deletion is incompatible with life. N-terminal truncation of DIDO (*Dido⊿NT*) provokes aneuploidy, centrosome amplification, and DNA damage in the form of centromere-localized breaks (Guerrero et al., 2010), and leads to chromosomal instability (Martinez-A and van Wely, 2011; Trachana et al., 2007). Mice with the *Dido⊿NT* mutation show hematological myeloid neoplasms, and alterations in DIDO are associated with the myelodysplastic syndrome in humans (Futterer et al., 2005). Characterization of *DIDO* isoform expression in myeloproliferative neoplasms showed no *DIDO2* expression differences in $CD34^+$ hematopoietic stem cells from polycythemia vera, essential thrombocythemia, and primary myelofibrosis patients. In contrast, *DIDO2* expression is high in advanced phases of chronic myeloid leukemia (Berzoti-Coelho et al., 2016), suggesting that DIDO2 contributes to this disease.

DIDO3 has a role in delivery of actin-dependent histone deacetylase 6 (HDAC6) to the primary cell cilium (Sanchez de Diego et al., 2014). HDAC6 counteracts the activity of α-tubulin acetyltransferase (ATAT1) (d'Ydewalle et al., 2011), which acetylates TUBULIN and thus stabilizes primary cilium architecture.

In a second mutation (*Dido3⊿CT*), we replaced the *Dido3*-specific last exon, which encodes its C terminus and includes the centrosomal targeting domain (Sanchez de Diego et al., 2014). Deletion of this region leads to embryonic lethality; embryos die by gestation day 8.5 (Futterer et al., 2012). ESCs derived from *Dido3⊿CT* mutant embryos do not differentiate correctly after aggregation and leukemia inhibitory factor (LIF) withdrawal, but retain their capacity for self-renewal, as shown by sustained expression of OCT4 and other markers of undifferentiated stem cells. Differentiation can be recovered in vitro by reconstitution with full-length DIDO3, retinoic acid (RA) treatment, or in the teratoma assay (Futterer et al., 2012). Ectopic expression of the common DIDO NT region in *Dido3⊿CT* cells downregulates stemness genes in EBs only when the wild-type (WT) PHD is present (Gatchalian et al., 2013). In vivo differentiation can be rescued by crossing *Dido3⊿CT* with the *Dido⊿NT* mutant. These double mutants overcome embryonic lethality, although the mice suffer high perinatal mortality and neurodevelopmental, morphogenetic, and metabolic alterations (Villares et al., 2015).

The DIDO1 isoform is upregulated when pro-B cells differentiate in vitro after growth factor starvation; its cytoplasmic localization requires phosphorylation and must be dephosphorylated for nuclear translocation (Garcia-Domingo et al., 1999, 2003). DIDO1 is also upregulated during WT ESC differentiation after LIF withdrawal and aggregation to EBs; this upregulation fails in mutant *Dido3⊿CT* ESCs (Futterer et al., 2012; Gatchalian et al., 2013).

Here we show an essential role for DIDO3 and DIDO1 isoforms at the onset of ESC differentiation. DIDO3 binds to its own promoter, associates with RNA polymerase II (RNA POL II), and regulates *Dido1* transcriptional activation; after binding to the H3K4me3 domain, DIDO1 helps to downregulate stemness genes and upregulate genes associated with ESC differentiation. Atypical protein kinase C (aPKC) phosphorylates the NT domain; in DIDO1, this causes its translocation to the outer layer of PE cells, where it associates with WWP2, an E3 ubiquitin-protein ligase, to promote degradation of OCT4, the master regulator of stemness. In DIDO3, this phosphorylation triggers translocation to the centrosome and promotes correct centrosome positioning. We describe a model by which, in ESC, self-regulating *Dido* splice variants participate in the early stages of developmentally controlled gene expression patterns that determine cell self-renewal versus differentiation.

RESULTS

Functional Effect of DIDO Domains on Regulation of Stemness Gene Expression

Dido3⊿CT ESCs are unable to differentiate correctly, and can serve as a model to study stem cell self-renewal and differentiation (Futterer et al., 2012). Here we used Agilent microarrays to compare transcriptomes of 10-day EBs (d10EBs) from WT and *Dido3⊿CT* cells. Gene ontology (GO) analysis showed persistent expression of stemness-related genes and genes involved in transcription regulation, and lack of genes associated with differentiation of all three germ layers (Figures 1 and S1; Tables S1 and S2).

To test the influence of distinct DIDO regions (Figure S2A), we expressed the common N-terminal part of DIDO (HA-DIDONT) or the missing specific C-terminal part of DIDO3 (HA-DIDO3CT) in *Dido3⊿CT* ESC, and compared the d10EB gene expression profile with that of WT EB. Ectopic HA-DIDONT expression partially restored gene expression to the WT EB pattern. As predicted from

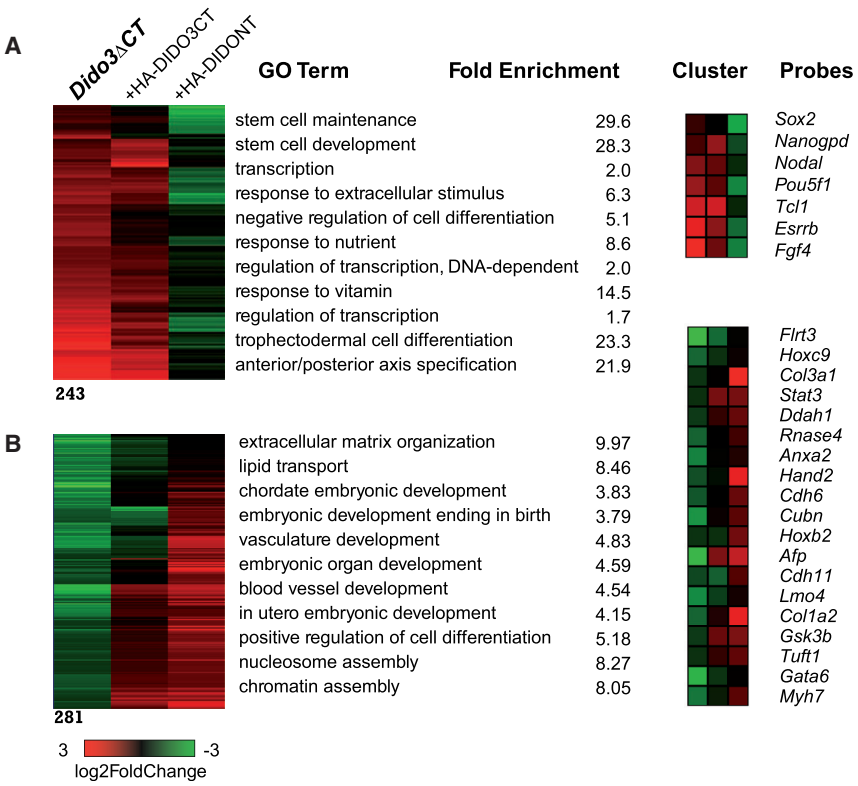

Figure 1. Functional Effect of DIDO Domain Expression in Day-10 Embryoid Bodies

(A) Group of genes, determined in Agilent microarrays, whose expression recovered to WT levels only after HA-DIDONT region expression in *Dido3ΔCT* ESCs, and GO analysis terms with example genes.

(B) Group of genes whose expression was fully recovered by HA-DIDONT and partially by the HA-DIDO3CT region, with GO analysis and example genes. All array data are from three biological replicates.

previous results, HA-DIDONT EBs recovered downregulation of stemness genes (Gatchalian et al., 2013) and expression of a subset of other genes; GO analysis indicated that these genes are involved in endoderm and mesoderm differentiation (Figures 1A and 1B). Genes associated with ectoderm differentiation were not rescued (Figure S1; Tables S1 and S2). In contrast, stemness-related genes were not downregulated by ectopic HA-DIDO3CT expression, and endoderm- and mesoderm-related gene expression were only partially restored (Figures 1A and 1B). Although the WT DIDO PHD domain is necessary for the restoration effect by the NT region (Gatchalian et al., 2013), it is not sufficient, as the NT must localize to the nucleus. In a mutant lacking the nuclear localization domain (HA-DIDONTΔNLS), the protein remained in cytoplasm (Figure S2B) and d10EBs showed no decrease in stemness-related genes (Figure S2C). These findings show the distinct effect of DIDONT and DIDO3CT domains on ESC differentiation, which led us to analyze the implication of the DIDO1 and DIDO3 isoforms in differentiation.

DIDO1 and DIDO3 Expression in Early ESC Differentiation Stages

In floating culture conditions, ESC aggregation to form EBs accompanied by LIF withdrawal leads EBs to mimic the early steps of in vivo cell differentiation (Desbaillets et al., 2000; Doetschman et al., 1985). By day 3–4, the outer cell layer of WT EB forms the PE, characterized by expression of endoderm markers such as GATA4 and by downregulation of OCT4, a major component of the ESC circuit responsible for self-renewal (Hamazaki et al., 2004; Niwa, 2010) (Figure 2A). Affymetrix microarray analysis showed differential gene expression between WT and *Dido3ΔCT* ESC. *Dido1* expression was 2.8-fold lower in *Dido3ΔCT* compared with WT ESCs (see Table S3 for full microarray data). At variance with WT EBs, *Dido3ΔCT* EBs did not correctly develop the PE cell layer (Figure 2A; Futterer et al., 2012) or induce increased *Dido1* expression (Gatchalian et al., 2013). We monitored DIDO1 and DIDO3 levels in WT d4EBs using antibodies to peptides of the specific DIDO1 or DIDO3 CT domains (PAB-DIDO1 and PAB-DIDO3) (Figures S3A and S3B). Whereas DIDO3 was expressed mainly in the nucleus, DIDO1 was found at the apical site of the PE cells, with weak nuclear expression (Figure 2B). Staining with the monoclonal MAB-1C6 antibody (generated against amino acids 2–90 of the common NT region) (Figure S2A) also showed DIDO nuclear staining, with faint expression at the apical membrane and limited co-localization with PAB-DIDO1 (see below).

A time-course analysis of DIDO1 expression during EB differentiation showed that, in contrast to *Dido3ΔCT*, WT

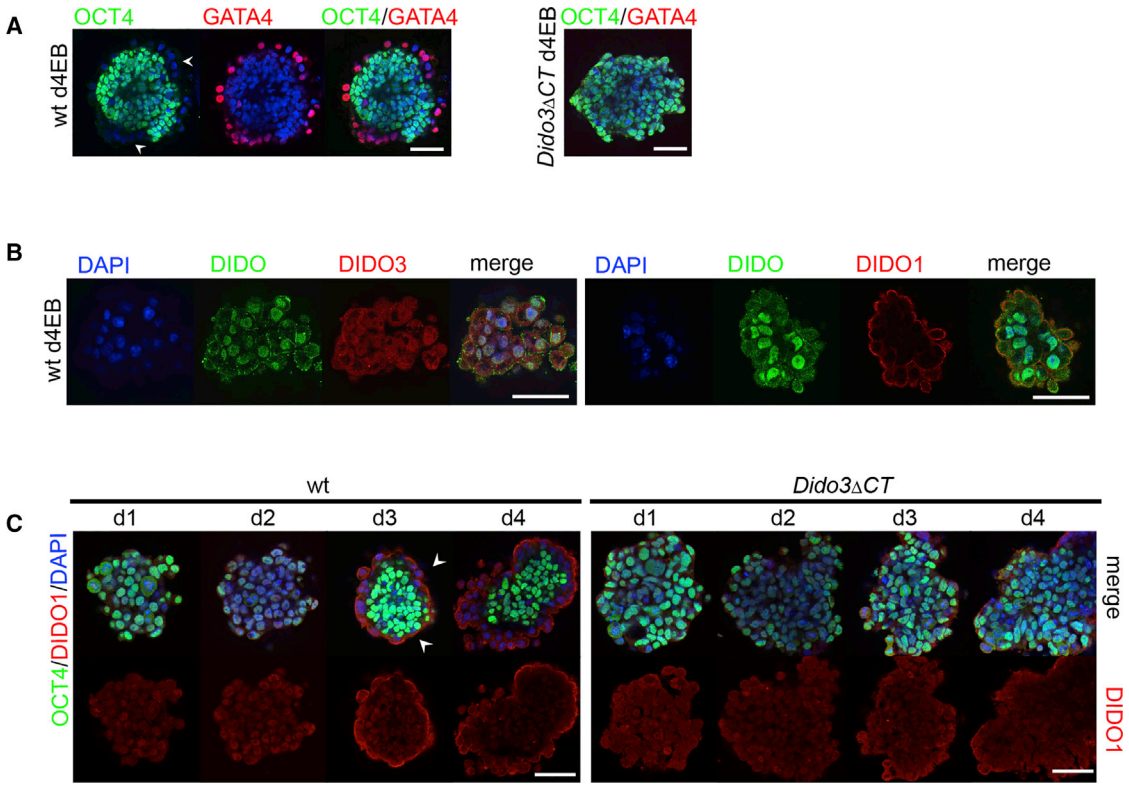

Figure 2. DIDO1 and DIDO3 Expression in Early ESC Differentiation

(A) Left: immunostaining of WT day-4 embryoid bodies (d4EBs) for OCT4 (green) and GATA4 (red); arrowheads mark outer primitive endoderm (PE) cell layer. Right: lack of PE formation in *Dido3ΔCT* d4EBs.

(B) Left: localization of DIDO isoforms using anti-DIDO MAB-1C6 (green; mainly in nucleus) and DIDO3-specific PAB-DIDO3 (red). Right: localization of DIDO isoforms using MAB-1C6 (green) and DIDO1-specific PAB-DIDO1 (red; preferentially at the apical membrane of outer cell layer).

(C) Left: developing PE and apical localization of DIDO1 (arrowheads) in a time course of WT d1–d4EBs labeled for OCT4 (green) and DIDO1 (red) expression. Right: lack of PE formation in a time course of *Dido3ΔCT* d1–d4EBs labeled for OCT4 (green) and DIDO1 (red).

All panels are confocal images with nuclear counterstaining (DAPI, blue). Scale bars, 50 μm.

EBs showed prominent apical membrane localization in PE cells starting at day 3 and persisting to day 4 (Figure 2C).

DIDO1 Is Essential for PE Development during EB Differentiation

To clarify the role of DIDO1 in ESC differentiation, we generated various WT ESC clones in which DIDO1 expression was inhibited by RNAi. Specificity control by RT-PCR showed a decrease in *Dido1*, but not in *Dido2* or *Dido3* RNA expression compared with small hairpin RNA (shRNA) *control*-infected cells (Figure S4A). DIDO1 protein reduction was also observed in cells expressing HA-DIDO1, as shown by western blot analysis (Figure S4B). shRNA-*Dido1* stable transfectants showed normal proliferation and self-renewal and were competent to form EBs. In contrast to shRNA-*control*, sh-*Dido1* EBs did not generate PE at day 4, as determined by absence of the PE markers GATA4 and FOXA2, OCT4 persistence (Figure 3A), and no apparent signs of differentiation beyond day 7 (Figure S4C). Moreover, RA treatment, which rescues PE formation and differentiation of *Dido3ΔCT* EBs (Figure 3B), failed to do so in shRNA-*Dido1* EBs (Figure 3C); FOXA2 staining was observed only inside the EBs and was independent of PE formation, as for WT EBs (Figure 3C).

DIDO1 upregulation and its apical expression in PE outer layer cells with concomitant OCT4 downregulation appeared to be essential during *Dido3ΔCT* EB differentiation induced by RA treatment or ectopic expression of HA-DIDO3 (Figure 3B). We also generated stable *Dido3ΔCT* ESC transfectants expressing HA-DIDO1, which proliferated normally in self-renewal conditions and showed no signs of differentiation (not shown). In the absence of LIF, EBs derived from these cells were able to reconstitute PE formation completely. In control staining, anti-HA

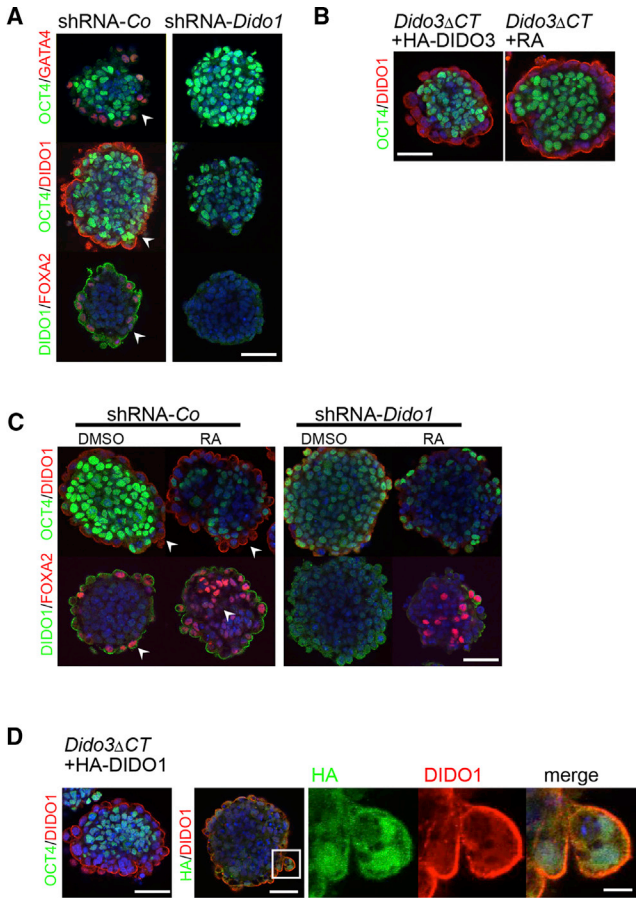

Figure 3. DIDO1 Is Essential for PE Formation

(A) (Left) shRNA-*Control* d4EBs with staining for PE formation (arrowheads). Top row: OCT4 (green; inside EBs), GATA4 (red; outer PE cells). Center: OCT4 (green; inside EBs) and DIDO1 (red; at apical membrane of outer PE cells). Bottom: DIDO1 (green; apical membrane) and FOXA4 (red; PE outer cell layer). (Right) All rows: lack of PE formation in shRNA-*Dido1* d4EBs.

(B) (Left) Reconstitution of PE formation by ectopic HA-DIDO3 expression in *Dido3ΔCT* d4EBs; OCT4 (green; inside EBs) and DIDO1 (red; at apical membrane of PE cells). (Right) The same PE reconstitution pattern of *Dido3ΔCT* d4EBs after retinoic acid (RA) treatment.

(C) Comparison of solvent (DMSO) versus RA-treated shRNA-*Co* d4EBs. (Left) Top: OCT4 (green; reduction inside EBs) and DIDO1 (red; at apical membrane of PE cells). Bottom: DIDO1 (green; at apical membrane of PE cells) and FOXA2 (red; arrowheads indicate PE outer layer in DMSO-treated cells and inside EBs in RA-treated cells). (Right) shRNA-*Dido1* d4EBs with lack of PE formation in DMSO- or RA-treated EBs, no DIDO1 labeling at apical membrane, and FOXA4 (red; only inside EBs).

(D) Ectopic HA-DIDO1 expression of reconstituted PE formation in *Dido3ΔCT* d4EBs. (Left) OCT4 (green; inside EBs) and DIDO1 (red; on apical membrane of PE cells). (Right) Co-localization of anti-HA (green) and DIDO1 (red) at apical membrane of outer PE cells.

Nuclei staining (DAPI, blue). Scale bars for EBs, 50 μm; Scale bar in boxed area of (D), 10 μm.

and anti-DIDO1 antibodies co-localized at the inner PE cell membrane, where DIDO1 is also located in WT EBs (Figure 3D).

Using qRT-PCR low-density arrays of representative genes related to undifferentiated stem cells or to differentiation to the three germ layers, we found that shRNA-*Dido1* EBs do not differentiate in vitro (Figure S4D). The gene expression pattern resembled that for *Dido3ΔCT* EBs (Figure S4E).

These data indicate that EBs require DIDO1 to generate the PE outer cell layer and initiate ESC differentiation. Furthermore, DIDO1 must translocate from the nucleus to cytoplasm for correct PE formation.

DIDO3 Regulates Cell Polarization and DIDO1 Acts as a Cell Lineage Marker during Asymmetric ESC Division

During ESC differentiation, a hallmark of differentiated PE cells is their apico-basolateral polarity (Doughton et al., 2014). To identify the role of DIDO in establishing polarization of the nascent PE layer in EBs, we used various polarization markers such as MEGALIN (Moore et al., 2014), F-ACTIN, aPKC (Bedzhov and Zernicka-Goetz, 2014), and acetylated TUBULIN (Quinones et al., 2011). In WT and shRNA-*control* EB, we confirmed PE cell polarization as detected by positive MEGALIN, F-ACTIN, and aPKC staining. We detected overlapping DIDO1 co-expression with these markers in the PE cell apical membrane. This was not the case in *Dido3ΔCT* or shRNA-*Dido1* EB, in which neither DIDO1 nor any of the polarization markers was found (Figure 4A). In the case of acetylated TUBULIN, expression was reduced only in *Dido3ΔCT* EB, whereas shRNA-*Dido1* EBs showed no difference compared with shRNA-*controls* (Figure 4A). These lower acetylation levels in *Dido3ΔCT* coincide with reported DIDO3 and HDAC6 association (Sanchez de Diego et al., 2014).

As PE outer layer formation is impaired in *Dido3ΔCT* and shRNA-*Dido1* EBs, we could not determine whether DIDO1 was responsible for PE cell polarization or whether lack of PE cells defined the absence of DIDO1. To address this question, we used a culture model of ESC rosettes established in Matrigel, in which polarization in central lumen of rosettes is independent of PE formation (Bedzhov and Zernicka-Goetz, 2014; Martin-Belmonte and Perez-Moreno, 2012). WT ESCs growing in Matrigel without LIF expressed MEGALIN, F-ACTIN, aPKC, and acetylated TUBULIN in the rosette central lumen. In *Dido3ΔCT* ESC, rosette polarization was severely impaired, since >60% of rosettes were abnormal, with aberrant staining patterns for all polarization markers including acetylated TUBULIN (Figure 4B). None of the rosettes from WT or *Dido3ΔCT* ESCs showed DIDO1 associated with polarization, which indicates that DIDO1 is dispensable in cell polarization.

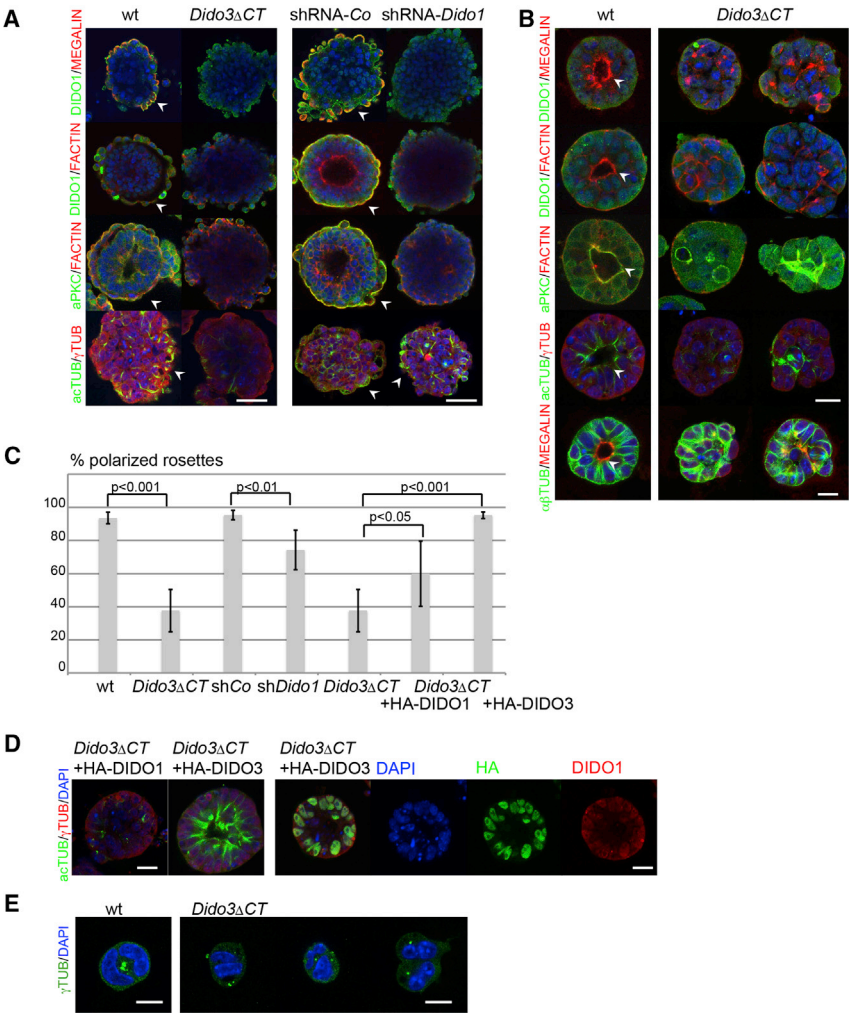

Figure 4. DIDO3 Regulates Polarization and DIDO1 Regulates Fate of PE Cells

(A) Left: comparison of WT and *Dido3ΔCT* d4EBs for apical polarization markers (MEGALIN, red; phalloidin-labeled F-ACTIN, red; aPKC, green; acetylated TUBULIN; green) and DIDO1 (green) at the PE layer (arrowheads). Right: comparison of shRNA-*control* and shRNA-*Dido1* d4EBs (staining as in left panel). Scale bars, 50 μm.

(B) Left: WT rosettes stained for polarization markers as in (A) and DIDO1 for apical polarization at the central lumen (arrowheads). Right: examples of *Dido3ΔCT* rosettes with mislocalization of polarization markers; bottom row of rosettes stained with anti-αβ-TUBULIN (green). Nuclei (DAPI, blue). Scale bars, 20 μm.

(C) Quantification of the percentage of polarized rosettes of WT, *Dido3ΔCT*, shRNA-*Co*, shRNA-*Dido1*, HA-DIDO1-reconstituted *Dido3ΔCT*, and HA-DIDO3-reconstituted *Dido3ΔCT*. Data are shown as mean ± SD (n from more than three independent experiments).

(D) Left: acetylated TUBULIN (green) in *Dido3ΔCT* rosettes reconstituted with HA-DIDO1 or HA-DIDO3. Right: HA-DIDO3 (green) and DIDO1 (red) localization in HA-DIDO3-reconstituted *Dido3ΔCT* rosettes. Scale bars, 20 μm.

(E) Position of centrosomes labeled with anti γ-TUBULIN (green) in WT (left) and *Dido3ΔCT* 2-cell stage rosettes (right). Nuclei (DAPI; blue). Scale bars, 10 μm.

Since TUBULIN acetylation has a role in microtubule dynamics and stabilization during cell polarization (Matsuyama et al., 2002), we studied microtubule and cytoskeleton organization in the rosettes. Based on quantification of acetylated and non-acetylated αβ-TUBULIN, we concluded that lower acetylated TUBULIN levels in *Dido3ΔCT* compared with WT rosettes and EBs were not the result of low TUBULIN levels (Figure S5A). Rosettes derived from *Dido3ΔCT*, in the presence of the HDAC6 inhibitors BML-281 (Kozikowski et al., 2008) or trichostatin A (Quinones et al., 2011), showed normal or even hyperacetylated TUBULIN compared with rosettes from WT ESCs (Figure S5B). Ectopic expression of HA-DIDO3, but not HA-DIDO1, completely normalized rosette polarization and TUBULIN acetylation in *Dido3ΔCT* rosettes, which showed that rescue of rosette polarization required DIDO3 but was less dependent on DIDO1 (Figure 4C). This polarization did not depend on DIDO1 or DIDO3 co-localization at the central lumen of rosettes (Figure 4D).

DIDO3 localizes to centrosomes and centrosomal organization is severely altered in *Dido* mutants (Futterer et al., 2012; Trachana et al., 2007), especially in the *Dido3ΔCT* mutant, in which the centrosomal targeting domain is absent (Sanchez de Diego et al., 2014). Since correct centrosome positioning is needed for single and central lumen initiation of rosettes (Rodriguez-Fraticelli et al., 2012; Taniguchi et al., 2015), we analyzed centrosome organization during polarization in early stages of rosette formation. Whereas at the 2-cell stage the large majority of centrosomes is correctly located in WT cells (<6.7% ± 2.1% are incorrect), a substantial percentage of centrosomes was incorrectly located in *Dido3ΔCT* cells (28.3% ± 2.1%) (Figure 4E). This centrosome mislocation in *Dido3ΔCT* cells coincides with defective aPKC, αβ-TUBULIN, and F-ACTIN expression as well as of EZRIN, a marker of lumen formation (Taniguchi et al., 2015) (Figure S5C).

These findings clearly show the relevance during cell polarization of DIDO3 compared with DIDO1, probably due

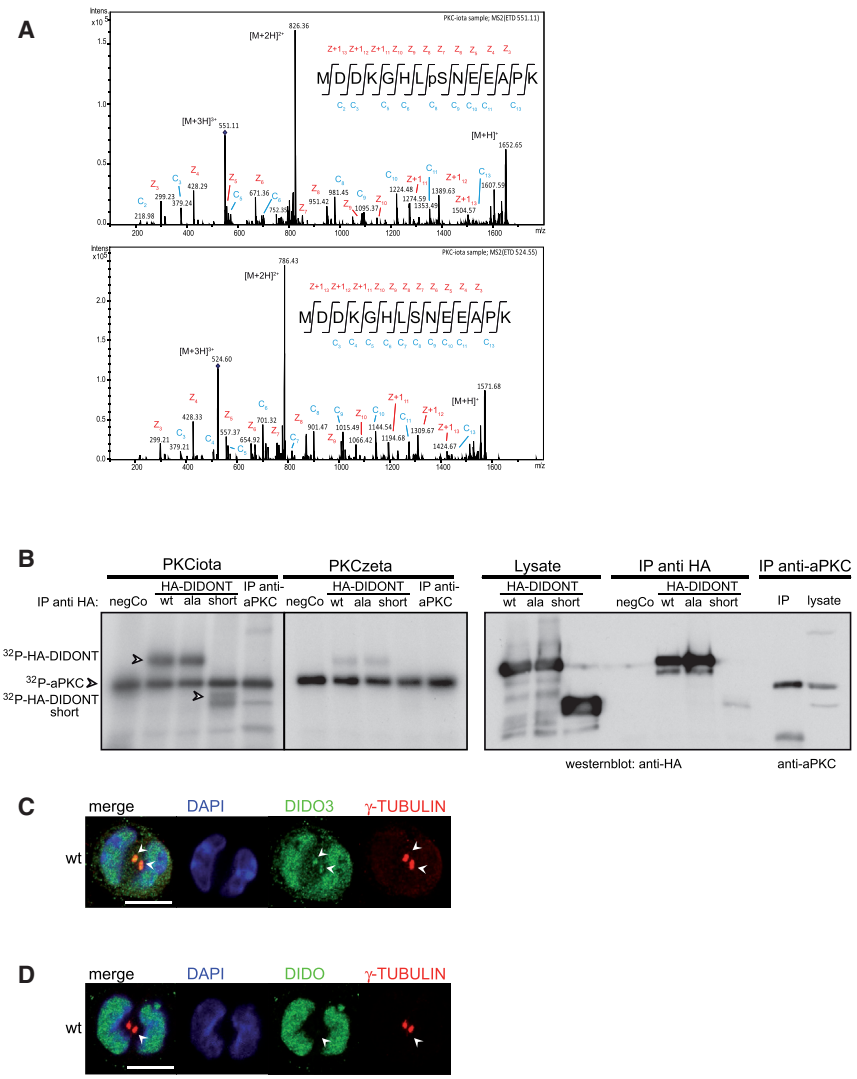

Figure 5. DIDO Associates with and Is Phosphorylated by PKCiota

(A) PKCiota phosphorylation of DIDO peptide MDDKGHLSNEEAPK on residue Ser8. Top: electron transfer dissociation (ETD) tandem mass spectrometry (MS/MS) spectrum of the *m/z* 551.1 ion corresponding to the phosphorylated peptide; pS indicates a phosphorylated serine residue. Bottom: ETD MS/MS spectrum of the *m/z* 524.5 ion corresponding to the non-phosphorylated peptide. Peptide sequences are shown with the identified c-/z-type ions.

(B) Left: anti-HA immunoprecipitates of a negative control, WT HA-DIDONT, HA-DIDONTSer8Ala, shortened HA-DIDONT, and anti-aPKC as positive control were used as substrates in an in vitro kinase assay with recombinant PKCiota and zeta; autoradiograph shows [^{32}P]ATP incorporation (arrowheads). Right: western blot controls of lysates and precipitates of corresponding proteins.

(C) Labeling of centrosomes (arrowheads) in WT 2-cell stage rosettes with γ-TUBULIN (red) and DIDO MAB-1C6 (green; nuclear only).

(D) Labeling of centrosomes (arrowheads) in WT 2-cell stage rosettes with PAB-DIDO3 (green) and γ-TUBULIN (red).

Scale bars: (C and D) 10 μm.

to its centrosomal location; centrosome misplacement in the *Dido3ΔCT* ESCs thus leads to formation of abnormal rosettes.

Translocation of DIDO1 to Cytoplasm and DIDO3 to the Centrosome Requires Association with and Phosphorylation by PKCiota

We found DIDO1 to be necessary for EBs to generate the PE outer cell layer, a process that requires DIDO1 translocation from the nucleus to cytoplasm. We identified DIDO1 at the PE cell apical membrane using the PAB-DIDO1 antibody, which recognizes phosphorylated and unphosphorylated DIDO1 forms. In EBs, the DIDONT-specific MAB-1C6 recognized DIDO1 and/or DIDO3 mainly in the nucleus, with faint expression at the PE inner membrane (Figure 2B). Epitope mapping and characterization of MAB-1C6 binding showed preferential reactivity with an unphosphorylated DIDO peptide (Figures S6A and S6B). We conclude that DIDO1 must be phosphorylated to localize at the PE apical membrane, which coincides with the finding that cytoplasmic DIDO1 is phosphorylated (Garcia-Domingo et al., 2003).

Tests for several markers on the polarized PE apical membrane showed localization of DIDO1 and aPKC (PKCiota and PKCzeta) (Figure 4A), both of which participate in cell polarization (Rosse et al., 2010). We analyzed the ability of both aPKCs to phosphorylate DIDO1 in an in vitro kinase assay with recombinant aPKC kinases that allow distinction between PKCiota and PKCzeta; as a substrate, we employed the same peptide used to characterize MAB-1C6 (Figure S6B). Mass spectrometry analysis (Navajas et al., 2011) showed that PKCiota phosphorylated the peptide at serine 8 (Figure 5A), as did PKCzeta to a lesser degree.

We tested whether recombinant PKCiota and/or PKCzeta phosphorylate WT HA-DIDONT, an HA-DIDONTSer8Ala mutant, or a shortened form of HA-DIDONT (cleaved at BglII) in an in vitro kinase assay with [γ-^{32}P]ATP. PKCiota and PKCzeta both phosphorylated WT HA-DIDONT and HA-DIDONTSer8Ala; again, PKCiota phosphorylation was higher (Figure 5B). Only PKCiota phosphorylated the shortened HA-DIDONT(BglII), whereas PKCzeta did not (Figure 5B). The results show that PKCiota phosphorylates the DIDONT and that serine 8 is not the only phosphorylation site. A possible functional correlation of PKCiota and the DIDO protein is supported by the similarity between *Dido3ΔCT* mutant and PKCiota knockout mouse phenotypes, since both mutations result in early embryonic lethality (Soloff et al., 2004), and ESCs derived from either mutant embryo do not differentiate correctly in vitro.

Like DIDO3, aPKC localizes to centrosomes (Atwood et al., 2013; Rosse et al., 2010), and DIDO3 is involved in organizing microtubules and polarization; we thus tested whether the DIDO3 NT region is also phosphorylated. Confocal analysis of 2-cell stage rosettes using PAB-DIDO3 and anti-γ-TUBULIN antibodies detected co-localization in the centrosome (Figure 5C). In contrast, MAB-1C6 and anti-γ-TUBULIN antibodies did not co-localize (Figure 5D), which suggests that centrosomal DIDO3 is also phosphorylated.

We concluded that phosphorylation of the DIDO1 and DIDO3 NT domains is a shared mechanism for DIDO translocation from the nucleus to cytoplasm (DIDO1) or to the centrosome (DIDO3), and suggest that the kinase PKCiota is involved in this process.

DIDO1 Interacts with WWP2 and Regulates OCT4 Degradation in PE Cells

When cultured in Matrigel, blastocyst inner mass cells generate rosettes and a polarized outer endoderm layer (Bedzhov et al., 2014). In these conditions, ESC-derived rosettes form this PE layer, albeit at much lower efficiency, as defined by GATA4 and DIDO1 expression and OCT4 downregulation (Figure S7A). As described above for EBs, we found no PE cell that co-expressed DIDO1 at the inner membrane and OCT4. Whereas OCT4 protein is not detected in these cells, they express *Oct4* RNA (Hamazaki et al., 2004), and OCT4 can be ubiquitinated by WWP2 (Liao and Jin, 2010; Xu et al., 2009). We thus tested for DIDO1 and WWP2 expression in PE from WT EBs, and found that they co-localized in PE cells (Figure 6A).

A western blot time-course analysis to monitor WWP2 expression during WT ESC differentiation showed the highest WWP2 expression in ESCs, which decreased during differentiation (Liao and Jin, 2010) (Figure S7B). WWP2 expression was lower in *Dido3ΔCT* than in WT ESCs, and its modification and downregulation were delayed during EB differentiation (Figure S7B). Using WWP2-specific antibody, we performed co-immunoprecipitation analyses in cells expressing HA-DIDO1, the HA-DIDONT domain, or HA-DIDO3CT. These studies confirmed interaction between HA-DIDO1 or HA-DIDONT and WWP2, whereas HA-DIDO3CT did not interact with WWP2 (Figure 6B). The results coincide with data in the BioGRID protein database that predict the DIDO and WWP2 interaction for *Homo sapiens*. Here we identify the DIDO NT domain as responsible for this interaction.

To define the cause of this WWP2/DIDO1 association, we used shRNA-*Wwp2* to inhibit WWP2 expression. Two representative clones were characterized as expressing different WWP2 levels (Figure S7C). Whereas shRNA-*control* EBs showed the predicted PE cell formation pattern (expressing FOXA2 and DIDO1 but not OCT4), shRNA-*Wwp2* clone A (trace WWP2 expression) did not develop PE (Figure 6C); this phenotype resembled shRNA-*Dido1* ESC or *Dido3ΔCT* ESC differentiation to EBs. In shRNA-*Wwp2* clone B, we observed PE formation in ~50% of EBs, with abnormal OCT4, DIDO1, and FOXA2 co-expression in these cells (Figure 6C). The results suggest that both DIDO1 and WWP2 are needed for correct PE formation, and that they associate and thus contribute to OCT4 ubiquitination and degradation.

DIDO3 Recruitment to Its Promoter and 3′ UTR Regions Regulates DIDO1 Expression

Since ectopic DIDO3 expression rescues the ability of these EBs to differentiate by upregulating DIDO1, we analyzed the mechanism underlying this upregulation. From HA-DIDO3-expressing *Dido3ΔCT* ESC, we prepared chromatin immunoprecipitation sequencing (ChIP-seq) immunoprecipitates with anti-HA antibodies and sequenced bound DNA fragments. Bioinformatics analysis showed that HA-DIDO3 binds to its own genomic locus at least on three regions (Figure 7A and Table S4) including the *Dido* proximal promoter, a site after the *Dido1* 3′ UTR region, and the *Dido3* 3′ UTR. The chromatin status of the *Dido* locus in mouse stem cells (data from Mouse ENCODE project; ENCODE Project Consortium, 2012) confirmed *Dido* as an actively transcribed gene in ESCs, as indicated by H3K4me3 and H3K9ac at the distal and proximal *Dido* promoters. The active elongation histone mark H3K36me3 was positive, whereas the heterochromatic silencing markers H3K27me3 and H3K9me3 were absent (Figure 7A).

Although no DNA binding motif has so far been identified for DIDO, the PHD of the common NT region binds to H3K4me3 (Gatchalian et al., 2013; Prieto et al., 2009). The peak detected in the proximal promoter is due to H3K4me3 binding, the only known binding site. There is no H3K4me3 at the second binding site (following the Dido1 3′ UTR), but rather H3K27ac, which is also present

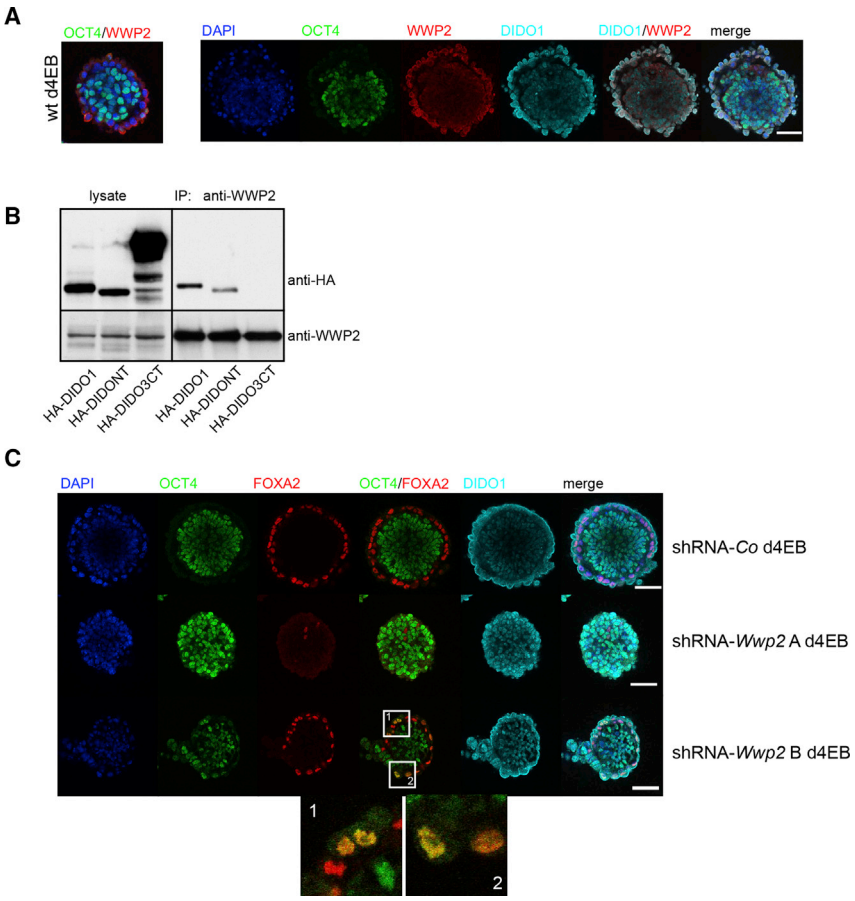

Figure 6. DIDO1 Interacts with WWP2 in PE Formation

(A) Left: WT d4EBs stain positive with anti-WWP2 (red) at apical membrane of OCT4 (green)-negative PE cells. Right: overlapping staining of DIDO1 (cyan) with WWP2 (red) on PE cells of WT d4EBs. Scale bar, 50 μm.

(B) WWP2 co-immunoprecipitated with HA-DIDO1 or HA-DIDONT, but not with HA-DIDO3CT.

(C) Co-staining of d4EBs with OCT4 (green) and PE markers FOXA2 (red) and DIDO1 (cyan) in WT d4EBs infected with shRNA-*Co* (top row) or two clones of shRNA-*Wwp2* A and B (center and bottom rows, respectively). Clone A completely lacked PE formation and clone B showed aberrant co-expression of OCT4 and FOXA2 in PE cells (zoomed images 1 and 2). Nuclei (DAPI, blue). Scale bars for EBs, 50 μm.

on both *Dido* promoters. This histone acetylation mark was described on poised enhancers that contribute to differentiation programs (Creyghton et al., 2010). H3K27ac was not detected as a DIDO binding site, but DIDO association to HDAC might participate in the H3K27 acetylation status.

As the DIDO TSFIIM domain is linked to RNA POL II (Rojas et al., 2005) and the yeast DIDO3 homolog BYE1 binds RNA POL II (Kinkelin et al., 2013; Pinskaya et al., 2014), we used co-immunoprecipitation experiments to test DIDO3 and DIDO3ΔCT association with RNA POL II. Both DIDO3 and DIDO3ΔCT associated with RNA POL II, which confirmed the link between DIDO and transcription (Figure 7B). When we included localization of RNA POL II, unphosphorylated or with various phosphorylation modifications (data from Brookes et al., 2012) in our representation of the *Dido* locus, we found RNA POL II peaks at DIDO3 ChIP-seq binding sites (Figure 7A).

To confirm DIDO3 and RNA POL II binding to the *Dido* locus, we performed further ChIP experiments followed by qPCR specific for the *Dido* proximal promoter and *Dido* internal binding site DNA, identified by ChIP-seq analysis. HA-DIDO3 (5.2-fold) and RNA POL II (6.5-fold) were enriched on the proximal promoter, as were HA-DIDO3 (3.8-fold) and RNA POL II (4.1-fold) on the internal *Dido* site (Figure 7C), which corroborates DIDO3 involvement in expression of *Dido* splice variants.

DISCUSSION

Advances in the identification and generation of stem cells from numerous organisms have produced vast knowledge in many fields including embryology and development. ESCs are capable of prolonged self-renewal in an undifferentiated state, but can also differentiate into several cell types. The molecular mechanisms that underlie these alternative processes remain to be identified, and appear critical for stem cell potential in regenerative/reparative medicine. Here we combined characterization of a stemness-associated locus (*Dido*) with the EBs' ability to mimic in vitro the early steps of in vivo ESC differentiation (Desbaillets et al., 2000; Doetschman et al., 1985).

ESC differentiation and formation of the PE cell layer require downregulation of stemness genes. In suspension culture, at 2–4 days after LIF deprivation, the polarized

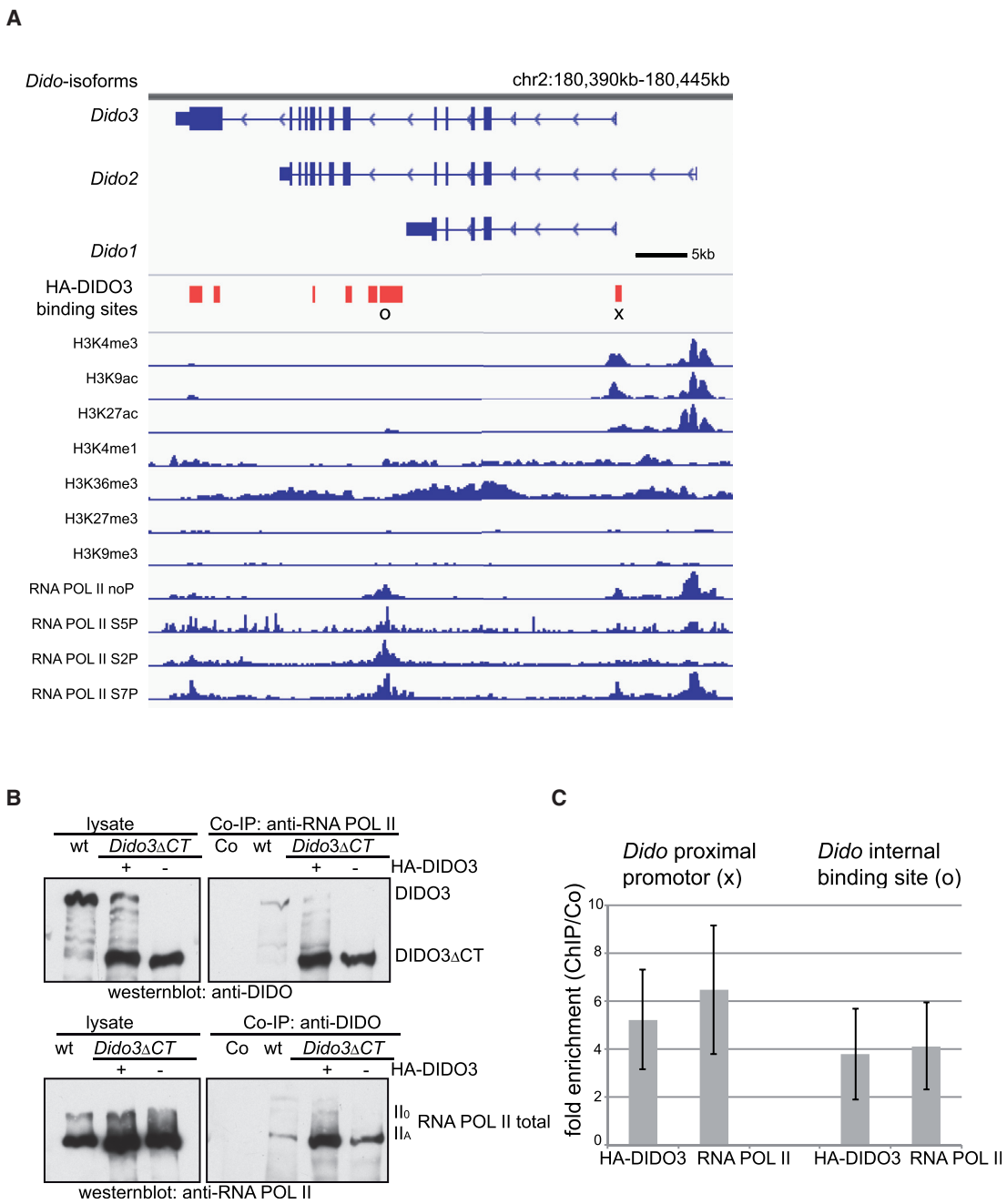

Figure 7. DIDO3 Binds to the *Dido* Gene and Interacts with RNA POL II

(A) Image of the 55-kb genomic region containing the three alternatively spliced isoforms of the *Dido* gene. HA-DIDO3 ChIP-seq binding sites (red boxes); chromatin status is reflected by individual tracks of histone modifications H3K4me3, H3K9ac, H3K27ac, H3K4me1, H3K36me3, H3K27me3, and H3K9me3 (ChIP-seq data from mouse ENCODE project); individual tracks from ChIP-seq data for RNA POL II unphosphorylated, Ser5, Ser2, or Ser7 phosphorylated (Brookes et al., 2012).

(B) Top: DIDO3, HA-DIDO3, and DIDO3ΔCT expression in lysates of WT, mutant ESCs reconstituted with HA-DIDO3, and mutant ESCs (left) and in anti-RNA POL II co-immunoprecipitates (right), developed with anti-DIDO (MAB-1C6). Bottom: expression of total RNA POL II in the same lysates (left) and in anti-DIDO co-immunoprecipitates (right), developed with anti-RNA POL II.

(C) qPCR data demonstrating x-fold ChIP enrichment for anti-HA-DIDO3 and -RNA POL II on *Dido* proximal promoter (right) and *Dido* internal sequence after *Dido1* 3′ UTR (left) relative to negative control (Co; immunoglobulin G), normalized to input amounts. Data are shown as mean ± SD (n from at least three independent experiments).

outer cell layer of EBs (the first cells to differentiate) forms the primitive endoderm, characterized by lack of stemness genes and expression of genes associated to the new PE cell fate. *Dido* is a gene complex that encodes three splice variants, *Dido1* (the smallest), *Dido2*, and *Dido3* (the largest) (Figure S3). We show that the DIDO1 isoform is a central player in regulating the EB switch from expansion to a differentiation/maintenance phase. During self-renewal, DIDO3 maintains stemness gene expression by binding to H3K4me3 and RNA POL II, and DIDO1 expression is repressed. Less is known of the role of DIDO2, the least-expressed isoform, which has only a few more amino acids than the DIDO3ΔCT mutant. We do not detect DIDO2 protein expression at differentiation onset, which is associated with changes in DIDO3/DIDO1.

Cell differentiation requires DIDO1 in cytoplasm and in the nucleus, where it probably competes with DIDO3 for binding to H3K4me3, promoting downregulation of stemness genes and DIDO3 degradation. Through its nuclear export signal, DIDO1 is exported to cytoplasm, which depends on its association to and phosphorylation by PKCiota (Figure 5). Once in the cytoplasm, DIDO1 associates to the E3 ubiquitin-protein ligase (WWP2), which leads to OCT4 ubiquitination and degradation (Figure 6). PKCiota also associates to and phosphorylates DIDO3 to form a complex that regulates correct centrosome positioning in daughter cells. DIDO3 interaction with HDAC6 (Sanchez de Diego et al., 2014) regulates TUBULIN acetylation, critical for its stabilization and dynamics (Figure 4). Both centrosome positioning and microtubule dynamics participate in the polarity pathway that controls stem cell self-renewal versus differentiation.

A model emerges in which DIDO acts as a switchboard that regulates a genetic program that drives stem cells between the transcription "modes" that operate to maintain pluripotency or promote differentiation. In these modes, control of the expression and cellular localization of different DIDO splice forms appears to be important. Whereas DIDO1 expression and phosphorylation commit cells to the first step in ESC differentiation, DIDO3 phosphorylation promotes its translocation to the centrosome, whose position it controls for the renewal or differentiation capacities of daughter cells.

Alternative mRNA isoforms are an important means of diversifying protein behavior, and have contributed to the complexity of vertebrate organisms (Roy et al., 2013). Here we show that two *Dido* isoforms generated by differential splicing are critical to determination of cell lineage early in ESC differentiation. Self-renewal and differentiation events apparently have distinct genetic requirements in the transcription modes for pluripotent ESCs and for differentiating cells, which must integrate all signals needed for each stage.

DIDO1 and DIDO3 have several mechanisms that might take part in the pluripotent and somatic cell transcription modes and in development. The composition of DIDO isoform domains might aid in establishing these modes. DIDO1 has the PHD, whereas DIDO3 encodes a much larger protein with three signature motifs, PHD, TFS2M, and SPOC, all typically found in proteins involved in transcription regulation. We found that DIDO3 binds RNA POL II and thus links DIDO to transcriptional control, as shown for the yeast DIDO homolog BYE1 (Kinkelin et al., 2013; Pinskaya et al., 2014). We show a direct DIDO3 role in regulating its own expression and that of DIDO1, as the *Dido3ΔCT* loss-of-function mutation confers a cell phenotype similar to that seen when DIDO1 is misregulated. ChIP mapping of DIDO3 recruitment to the *Dido* locus also indicated a binding pattern associated with a region that includes, but is not limited to, the *Dido* promoter (Figure 7). Results from chromatin binding indicated that DIDO3 binding to its own genomic DNA modulates *Dido1* expression and might participate in regulating core stemness genes, a question currently under study. These findings coincide with the role of d(PPS), the DIDO homolog in *Drosophila*. d(PPS) protein also has four signature motifs typically found in proteins that act in transcriptional regulation; d(PPS) is needed to regulate *Sxl* (*sex-lethal*) splicing (Johnson et al., 2010) and DIDO3 is necessary for DIDO1 expression. Given the known d(PPS) splicing function, our data and the parallels with d(PPS) results suggest a role for DIDO in transcription control by splicing.

EXPERIMENTAL PROCEDURES

Cell Culture and Transfection

All experiments using animal materials were designed in compliance with European Union legislation and approved by the Committee for Ethics in Animal Experimentation of the Centro Nacional de Biotecnología (CNB/CSIC) (Proex 322/15).

Mouse ESCs were maintained in KO-DMEM (Gibco, Invitrogen) with 20% fetal calf serum, 1× Glutamax (Invitrogen), non-essential amino acids, 0.05 mM 2-mercaptoethanol, 100 U/mL penicillin, 0.1 mg/mL streptomycin, and 1,000 U/mL mouse LIF supplement (Millipore) on a layer of mitomycin C-treated mouse embryonic fibroblasts or gelatinized tissue culture plates.

EBs were formed and cultured in suspension conditions in low-attachment dishes in the same medium without LIF. Rosettes were formed in the same medium without LIF and 5% Matrigel (Becton Dickinson) on 8-well chamber slides (iBidi) coated with 25 μL of Matrigel per well for 3 days, or 1 day for 2-cell stages.

Cells were transfected with Lipofectamine 2000 (Invitrogen) according to the manufacturer's protocols. For overexpression experiments, *Dido1*, *Dido3*, or *Dido* fragments were cloned in mammalian expression vector pCAGG-HA-tagged *Dido*-IRES-puromycin resistance cassette.

For shRNA *Dido1* experiments, we used *Dido1*-specific and negative control GIPZ lentiviral particles (Thermo Scientific). For *Wwp2* shRNA, we used retroviral pGFP-V-RS vector with control or four different 29mer shRNAs to murine *Wwp2* (Origene). Stable transfectants were obtained in all cases by puromycin selection (1 μg/mL). For target sequences, see Supplemental Experimental Procedures.

Immunofluorescence

ESC, EB, or rosettes were fixed in 4% formaldehyde, permeabilized with 0.2% NP-40, blocked with 1% BSA, and stained with primary (overnight, 4°C) and secondary antibodies (2 hr, room temperature) and DAPI (30 min, room temperature). For the list of antibodies, see Supplemental Experimental Procedures.

A Zeiss laser scanning confocal microscope was used for confocal microscopy; images were processed with ImageJ software (NIH).

Immunoprecipitation

For co-immunoprecipitation, cells were lysed in NETN buffer (20 mM HEPES [pH 7.5], 300 mM NaCl, 0.5 mM EDTA, 10% glycerol, 0.5% NP-40) with protease inhibitor cocktail (Roche) and 1 mM PMSF; cells for immunoprecipitation were lysed in RIPA buffer with the same inhibitors. Lysates were immunoprecipitated with specific antibody (overnight, 4°C), followed by addition of magnetic beads (Dynabeads, Invitrogen) coupled to Protein A or Protein G1, depending on the species and isotype of the first capture antibody. Immunoprecipitates were washed six times and released from beads in sample buffer (10 min, 70°C).

Western Blot

Samples were separated by 4%–10% SDS-PAGE depending on protein size, then transferred to nitrocellulose membrane (Bio-Rad), followed by western blot analysis with indicated antibodies. ECL solution (PerkinElmer) was used to visualize proteins.

Microarray and qRT-PCR

Total RNA was prepared with TRIzol (Invitrogen) and used for qRT-PCR in low-density arrays (TaqMan mouse stem cell, Applied Biosystems) and microarrays. Samples were labeled and hybridized on the mouse genome 430 2.0 array (Affymetrix) or Mouse GE 4x44K v2 microarrays (Agilent); three biological replicates were used for all conditions.

For detailed methods, see Supplemental Experimental Procedures.

Kinase Assay

Purified immunoprecipitates (magnetic beads with bound anti-HA + HA-DIDO1 or anti-HA + HA-DIDONT fragments) were washed once in kinase buffer (50 mM Tris [pH 7.5], 20 mM $MgCl_2$, 10 mM $MnCl_2$). Labeling reactions were performed with 10 μL of precipitated mixture +10 μL of recombinant PKC +5 μL of ATP-mix (cold ATP +10 μCi [γ-^{32}P]ATP) (30 min, 30°C), washed twice in kinase buffer, released in sample buffer (10 min, 70°C) and resolved on a gel. The gel was fixed in methanol/acetic acid, dried, and exposed to X-ray film. Enzymes used were recombinant human PKCiota (14-505, Merck Millipore; 0.5 μg/reaction) and recombinant human PKCzeta (14-525, Merck Millipore; 0.2 μg/reaction).

Phosphopeptide Analysis

Phosphopeptides were analyzed by liquid chromatography-tandem mass spectrometry ion trap, alternating collision-induced dissociation, and electron transfer dissociation fragmentation techniques. For details, see Supplemental Experimental Procedures.

Chromatin Immunoprecipitation and qPCR

For ChIP, we used the MAGnify Chromatin Immunoprecipitation System (Invitrogen) according to the manufacturer's protocol, with overnight immunoprecipitate incubation at 4°C. Inputs and eluates were used for qPCR with SYBR Green in an ABI PRISM 7900HT PCR (Applied Biosystems); x-fold probe enrichment was calculated relative to immunoglobulin G control precipitates, normalized to inputs. For primers, see Supplemental Experimental Procedures.

Chromatin Immunoprecipitation Sequencing

ChIP-seq was performed mainly as described by O'Geen et al. (2010). In brief, HA-DIDO3-expressing *Dido3ΔCT* ESCs were 1% formaldehyde-fixed and lysed in lysis buffer with proteinase inhibitor cocktail (Roche) and PMSF. Chromatin was sonicated in a Diagenode Bioruptor; fragments of ~200–500 base pairs (verified by gel) were diluted with RIPA buffer and precipitated with anti-HA polyclonal antibody (ChIP-grade, ab9110; Abcam) coupled to magnetic beads coated with anti-rabbit immunoglobulin (Invitrogen; overnight, 4°C). Beads were washed extensively, and the precipitates were eluted and reverse-crosslinked; the DNA was purified on Qiagen columns. Further processing and massive sequencing was performed by the Genomics Service Unit, Parque Científico de Madrid (see Supplemental Experimental Procedures).

ChIP-Seq Analysis

Mapped reads were aligned with the Bowtie program on the mouse genome (NCBI Build 37/UCSC mm9) and significant peaks identified using MACS software (v. 1.4) with default thresholds. For detailed procedures, see Supplemental Experimental Procedures.

Statistical Analysis

Data are shown as mean ± SD. Statistical analyses were performed using Student's t test.

ACCESSION NUMBERS

The accession number for all genomic data (Affymetrix and Agilent microarrays, ChIP-seq) reported in this paper is GEO: GSE85029.

SUPPLEMENTAL INFORMATION

Supplemental Information includes Supplemental Experimental Procedures, seven figures, and four tables and can be found with this article online at http://dx.doi.org/10.1016/j.stemcr.2017.02.013.

AUTHOR CONTRIBUTIONS

A.F. designed, performed, and analyzed most of the experiments and co-wrote the paper. J.d.C. analyzed the transciptome and

ChIP-seq data and co-wrote the paper. R.N., L.A., and J.G. performed and analyzed some experiments. A.T.-G. and C.P.-B. provided reagents. I.B. and F.M.-B. provided rosette technology, expertise, and feedback. C.M.-A. conceptualized experiments, analyzed data, co-wrote the paper, and secured funding.

ACKNOWLEDGMENTS

We thank the CNB Proteomics facility for peptide synthesis, the CNB Genomic Service Unit for performing microarray experiments, and C. Mark for editorial assistance. This work was supported by grants from the Spanish Ministerio de Economía y Competitividad (MINECO-FEDER SAF2013-42289-R and SAF2016-75456-R) and the Alfonso Martín Escudero Foundation.

Received: September 28, 2016
Revised: February 15, 2017
Accepted: February 16, 2017
Published: March 16, 2017

REFERENCES

Atwood, S.X., Li, M., Lee, A., Tang, J.Y., and Oro, A.E. (2013). GLI activation by atypical protein kinase C iota/lambda regulates the growth of basal cell carcinomas. Nature *494*, 484–488.

Bedzhov, I., and Zernicka-Goetz, M. (2014). Self-organizing properties of mouse pluripotent cells initiate morphogenesis upon implantation. Cell *156*, 1032–1044.

Bedzhov, I., Leung, C.Y., Bialecka, M., and Zernicka-Goetz, M. (2014). In vitro culture of mouse blastocysts beyond the implantation stages. Nat. Protoc. *9*, 2732–2739.

Berzoti-Coelho, M.G., Ferreira, A.F., de Souza Nunes, N., Pinto, M.T., Junior, M.C., Simoes, B.P., Martinez, A.C., Souto, E.X., Panepucci, R.A., Covas, D.T., et al. (2016). The expression of Death Inducer-Obliterator (DIDO) variants in myeloproliferative neoplasms. Blood Cells Mol. Dis. *59*, 25–30.

Brandenberger, R., Wei, H., Zhang, S., Lei, S., Murage, J., Fisk, G.J., Li, Y., Xu, C., Fang, R., Guegler, K., et al. (2004). Transcriptome characterization elucidates signaling networks that control human ES cell growth and differentiation. Nat. Biotechnol. *22*, 707–716.

Brookes, E., de Santiago, I., Hebenstreit, D., Morris, K.J., Carroll, T., Xie, S.Q., Stock, J.K., Heidemann, M., Eick, D., Nozaki, N., et al. (2012). Polycomb associates genome-wide with a specific RNA polymerase II variant, and regulates metabolic genes in ESCs. Cell Stem Cell *10*, 157–170.

Chen, X., Xu, H., Yuan, P., Fang, F., Huss, M., Vega, V.B., Wong, E., Orlov, Y.L., Zhang, W., Jiang, J., et al. (2008). Integration of external signaling pathways with the core transcriptional network in embryonic stem cells. Cell *133*, 1106–1117.

Creyghton, M.P., Cheng, A.W., Welstead, G.G., Kooistra, T., Carey, B.W., Steine, E.J., Hanna, J., Lodato, M.A., Frampton, G.M., Sharp, P.A., et al. (2010). Histone H3K27ac separates active from poised enhancers and predicts developmental state. Proc. Natl. Acad. Sci. USA *107*, 21931–21936.

d'Ydewalle, C., Krishnan, J., Chiheb, D.M., Van Damme, P., Irobi, J., Kozikowski, A.P., Vanden Berghe, P., Timmerman, V., Robberecht, W., and Van Den Bosch, L. (2011). HDAC6 inhibitors reverse axonal loss in a mouse model of mutant HSPB1-induced Charcot-Marie-Tooth disease. Nat. Med. *17*, 968–974.

Desbaillets, I., Ziegler, U., Groscurth, P., and Gassmann, M. (2000). Embryoid bodies: an in vitro model of mouse embryogenesis. Exp. Physiol. *85*, 645–651.

Doetschman, T.C., Eistetter, H., Katz, M., Schmidt, W., and Kemler, R. (1985). The in vitro development of blastocyst-derived embryonic stem cell lines: formation of visceral yolk sac, blood islands and myocardium. J. Embryol. Exp. Morphol. *87*, 27–45.

Doughton, G., Wei, J., Tapon, N., Welham, M.J., and Chalmers, A.D. (2014). Formation of a polarised primitive endoderm layer in embryoid bodies requires fgfr/erk signalling. PLoS One *9*, e95434.

ENCODE Project Consortium (2012). An integrated encyclopedia of DNA elements in the human genome. Nature *489*, 57–74.

Futterer, A., Campanero, M.R., Leonardo, E., Criado, L.M., Flores, J.M., Hernandez, J.M., San Miguel, J.F., and Martinez, A.C. (2005). Dido gene expression alterations are implicated in the induction of hematological myeloid neoplasms. J. Clin. Invest. *115*, 2351–2362.

Futterer, A., Raya, A., Llorente, M., Izpisua-Belmonte, J.C., de la Pompa, J.L., Klatt, P., and Martinez, A.C. (2012). Ablation of Dido3 compromises lineage commitment of stem cells in vitro and during early embryonic development. Cell Death Differ. *19*, 132–143.

Garcia-Domingo, D., Leonardo, E., Grandien, A., Martinez, P., Albar, J.P., Izpisua-Belmonte, J.C., and Martinez, A.C. (1999). DIO-1 is a gene involved in onset of apoptosis in vitro, whose misexpression disrupts limb development. Proc. Natl. Acad. Sci. USA *96*, 7992–7997.

Garcia-Domingo, D., Ramirez, D., Gonzalez de Buitrago, G., and Martinez, A.C. (2003). Death inducer-obliterator 1 triggers apoptosis after nuclear translocation and caspase upregulation. Mol. Cell Biol. *23*, 3216–3225.

Gatchalian, J., Futterer, A., Rothbart, S.B., Tong, Q., Rincon-Arano, H., Sanchez de Diego, A., Groudine, M., Strahl, B.D., Martinez, A.C., van Wely, K.H., et al. (2013). Dido3 PHD modulates cell differentiation and division. Cell Rep. *4*, 148–158.

Guerrero, A.A., Gamero, M.C., Trachana, V., Futterer, A., Pacios-Bras, C., Diaz-Concha, N.P., Cigudosa, J.C., Martinez, A.C., and van Wely, K.H. (2010). Centromere-localized breaks indicate the generation of DNA damage by the mitotic spindle. Proc. Natl. Acad. Sci. USA *107*, 4159–4164.

Hamazaki, T., Oka, M., Yamanaka, S., and Terada, N. (2004). Aggregation of embryonic stem cells induces Nanog repression and primitive endoderm differentiation. J. Cell Sci. *117*, 5681–5686.

Johnson, M.L., Nagengast, A.A., and Salz, H.K. (2010). PPS, a large multidomain protein, functions with sex-lethal to regulate alternative splicing in Drosophila. PLoS Genet. *6*, e1000872.

Kettenberger, H., Armache, K.J., and Cramer, P. (2003). Architecture of the RNA polymerase II-TFIIS complex and implications for mRNA cleavage. Cell *114*, 347–357.

Kidder, B.L., Yang, J., and Palmer, S. (2008). Stat3 and c-Myc genome-wide promoter occupancy in embryonic stem cells. PLoS One *3*, e3932.

Kim, J., Chu, J., Shen, X., Wang, J., and Orkin, S.H. (2008). An extended transcriptional network for pluripotency of embryonic stem cells. Cell *132*, 1049–1061.

Kinkelin, K., Wozniak, G.G., Rothbart, S.B., Lidschreiber, M., Strahl, B.D., and Cramer, P. (2013). Structures of RNA polymerase II complexes with Bye1, a chromatin-binding PHF3/DIDO homologue. Proc. Natl. Acad. Sci. USA *110*, 15277–15282.

Kozikowski, A.P., Tapadar, S., Luchini, D.N., Kim, K.H., and Billadeau, D.D. (2008). Use of the nitrile oxide cycloaddition (NOC) reaction for molecular probe generation: a new class of enzyme selective histone deacetylase inhibitors (HDACIs) showing picomolar activity at HDAC6. J. Med. Chem. *51*, 4370–4373.

Liao, B., and Jin, Y. (2010). Wwp2 mediates Oct4 ubiquitination and its own auto-ubiquitination in a dosage-dependent manner. Cell Res. *20*, 332–344.

Martin-Belmonte, F., and Perez-Moreno, M. (2012). Epithelial cell polarity, stem cells and cancer. Nat. Rev. Cancer *12*, 23–38.

Martinez-A, C., and van Wely, K.H. (2011). Centromere fission, not telomere erosion, triggers chromosomal instability in human carcinomas. Carcinogenesis *32*, 796–803.

Matsuyama, A., Shimazu, T., Sumida, Y., Saito, A., Yoshimatsu, Y., Seigneurin-Berny, D., Osada, H., Komatsu, Y., Nishino, N., Khochbin, S., et al. (2002). In vivo destabilization of dynamic microtubules by HDAC6-mediated deacetylation. EMBO J. *21*, 6820–6831.

Moore, R., Tao, W., Meng, Y., Smith, E.R., and Xu, X.X. (2014). Cell adhesion and sorting in embryoid bodies derived from N- or E-cadherin deficient murine embryonic stem cells. Biol. Open *3*, 121–128.

Musselman, C.A., and Kutateladze, T.G. (2011). Handpicking epigenetic marks with PHD fingers. Nucleic Acids Res. *39*, 9061–9071.

Navajas, R., Paradela, A., and Albar, J.P. (2011). Immobilized metal affinity chromatography/reversed-phase enrichment of phosphopeptides and analysis by CID/ETD tandem mass spectrometry. Methods Mol. Biol. *681*, 337–348.

Niwa, H. (2007). How is pluripotency determined and maintained? Development *134*, 635–646.

Niwa, H. (2010). Mouse ES cell culture system as a model of development. Dev. Growth Differ. *52*, 275–283.

Noatynska, A., Tavernier, N., Gotta, M., and Pintard, L. (2013). Coordinating cell polarity and cell cycle progression: what can we learn from flies and worms? Open Biol. *3*, 130083.

O'Geen, H., Frietze, S., and Farnham, P.J. (2010). Using ChIP-seq technology to identify targets of zinc finger transcription factors. Methods Mol. Biol. *649*, 437–455.

Pinskaya, M., Ghavi-Helm, Y., Mariotte-Labarre, S., Morillon, A., Soutourina, J., and Werner, M. (2014). PHD and TFIIS-Like domains of the Bye1 transcription factor determine its multivalent genomic distribution. PLoS One *9*, e102464.

Prieto, I., Kouznetsova, A., Futterer, A., Trachana, V., Leonardo, E., Alonso Guerrero, A., Cano Gamero, M., Pacios-Bras, C., Leh, H., Buckle, M., et al. (2009). Synaptonemal complex assembly and H3K4Me3 demethylation determine DIDO3 localization in meiosis. Chromosoma *118*, 617–632.

Quinones, G.B., Danowski, B.A., Devaraj, A., Singh, V., and Ligon, L.A. (2011). The posttranslational modification of tubulin undergoes a switch from detyrosination to acetylation as epithelial cells become polarized. Mol. Biol. Cell *22*, 1045–1057.

Rodriguez-Fraticelli, A.E., Auzan, M., Alonso, M.A., Bornens, M., and Martin-Belmonte, F. (2012). Cell confinement controls centrosome positioning and lumen initiation during epithelial morphogenesis. J. Cell Biol. *198*, 1011–1023.

Rojas, A.M., Sanchez-Pulido, L., Futterer, A., van Wely, K.H., Martinez, A.C., and Valencia, A. (2005). Death inducer obliterator protein 1 in the context of DNA regulation. Sequence analyses of distant homologues point to a novel functional role. FEBS J. *272*, 3505–3511.

Rosse, C., Linch, M., Kermorgant, S., Cameron, A.J., Boeckeler, K., and Parker, P.J. (2010). PKC and the control of localized signal dynamics. Nat. Rev. Mol. Cell Biol. *11*, 103–112.

Roy, B., Haupt, L.M., and Griffiths, L.R. (2013). Review: alternative splicing (AS) of genes as an approach for generating protein complexity. Curr. Genomics *14*, 182–194.

Sanchez de Diego, A., Alonso Guerrero, A., Martinez-A, C., and van Wely, K.H. (2014). Dido3-dependent HDAC6 targeting controls cilium size. Nat. Commun. *5*, 3500.

Sanchez-Pulido, L., Rojas, A.M., van Wely, K.H., Martinez, A.C., and Valencia, A. (2004). SPOC: a widely distributed domain associated with cancer, apoptosis and transcription. BMC Bioinformatics *5*, 91.

Soloff, R.S., Katayama, C., Lin, M.Y., Feramisco, J.R., and Hedrick, S.M. (2004). Targeted deletion of protein kinase C lambda reveals a distribution of functions between the two atypical protein kinase C isoforms. J. Immunol. *173*, 3250–3260.

Taniguchi, K., Shao, Y., Townshend, R.F., Tsai, Y.H., DeLong, C.J., Lopez, S.A., Gayen, S., Freddo, A.M., Chue, D.J., Thomas, D.J., et al. (2015). Lumen formation is an intrinsic property of isolated human pluripotent stem cells. Stem Cell Rep. *5*, 954–962.

Trachana, V., van Wely, K.H., Guerrero, A.A., Futterer, A., and Martinez-A, C. (2007). Dido disruption leads to centrosome amplification and mitotic checkpoint defects compromising chromosome stability. Proc. Natl. Acad. Sci. USA *104*, 2691–2696.

Villares, R., Gutierrez, J., Futterer, A., Trachana, V., Gutierrez del Burgo, F., and Martinez, A.C. (2015). Dido mutations trigger perinatal death and generate brain abnormalities and behavioral alterations in surviving adult mice. Proc. Natl. Acad. Sci. USA *112*, 4803–4808.

Xu, H., Wang, W., Li, C., Yu, H., Yang, A., Wang, B., and Jin, Y. (2009). WWP2 promotes degradation of transcription factor OCT4 in human embryonic stem cells. Cell Res. *19*, 561–573.

Stem Cell Reports, Volume *8*

Supplemental Information

DIDO as a Switchboard that Regulates Self-Renewal and Differentiation in Embryonic Stem Cells

Agnes Fütterer, Jésus de Celis, Rosana Navajas, Luis Almonacid, Julio Gutiérrez, Amaia Talavera-Gutiérrez, Cristina Pacios-Bras, Ilenia Bernascone, Fernando Martin-Belmonte, and Carlos Martinéz-A

Supplemental Information

Supplemental Figures

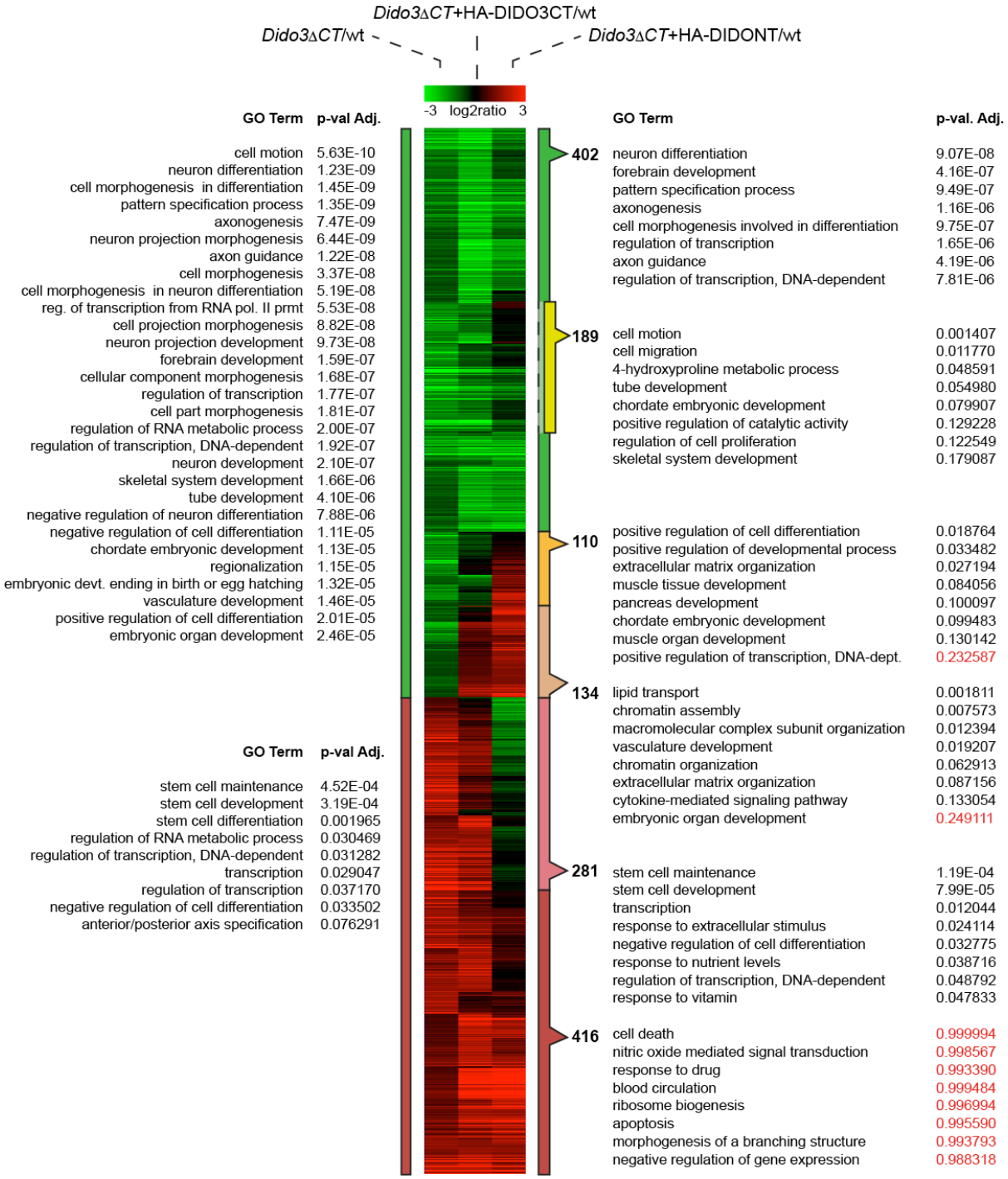

Figure S1. ***Functional effect of DIDO domain expression in Dido3ΔCT day 10 embryoid bodies (d10EB).*** **Related to Figure 1.** Complete results and GO analysis of Agilent microarray data for d10EB from *Dido3ΔCT* (left), *Dido3ΔCT*+HA-DIDO3CT (center) and *Dido3ΔCT*+HA-DIDONT (right) cells vs wt.

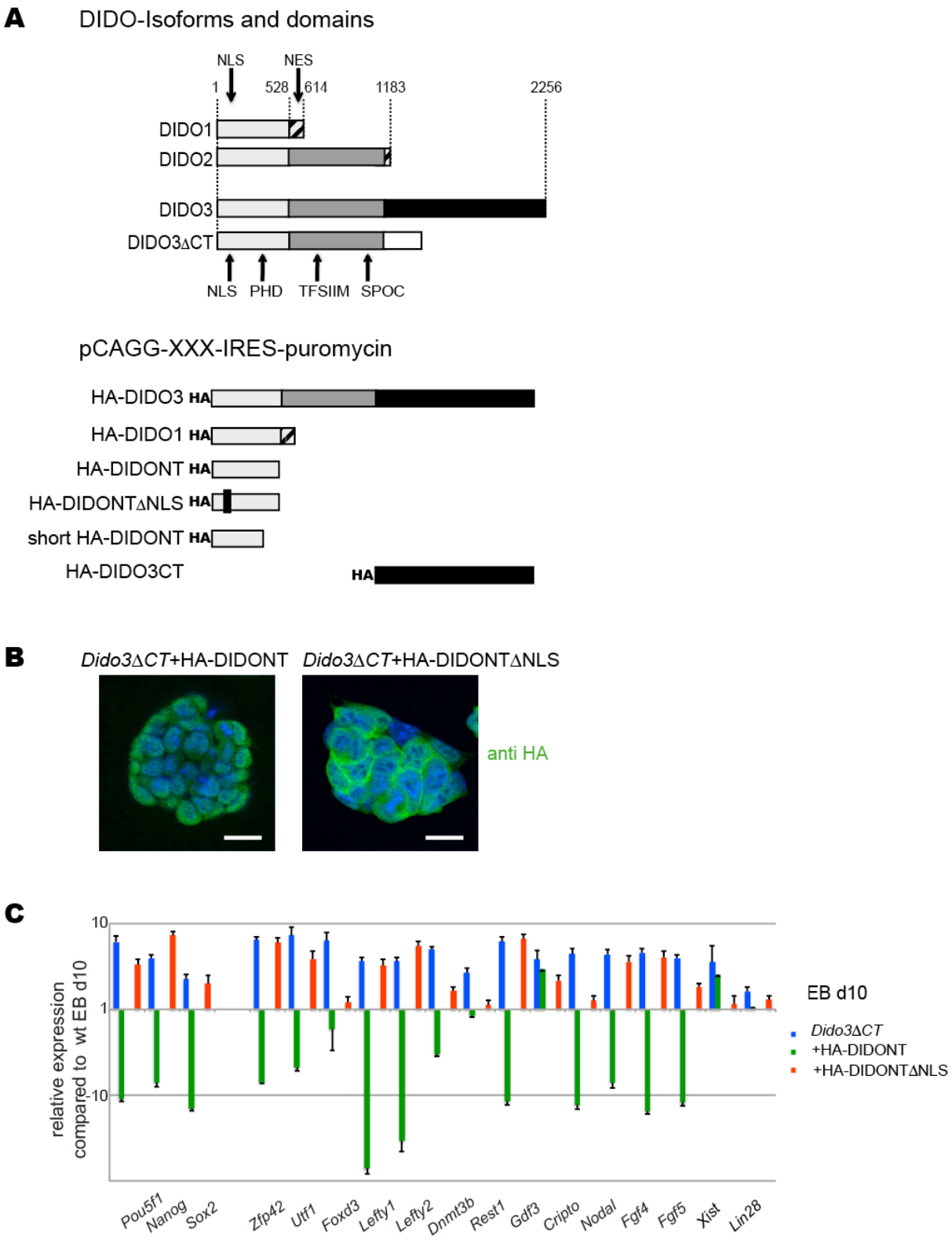

Figure S2. ***Scheme of DIDO domains and expression vectors and effect of HA-DIDONTΔNLS expression on Dido3ΔCT day 10 embryoid bodies (d10EB).*** **Related to Figure 1.** (**A**) Top, scheme of DIDO isoforms and their conserved domains, nuclear localization site (NLS) and nuclear export signal (NES). Bottom, HA-tagged plasmids used for ectopic expression of DIDO regions. (**B**) Top, labeling of embryonic stem cells (ESC) with anti-HA (green) for cellular localization of HA-DIDONT (nucleus) vs HA-DIDONTΔNLS (cytoplasm). Nuclear counterstaining (DAPI, blue). Scale bars, 20 μm. (**C**) Bottom, relative expression compared to wt (baseline) of selected stemness markers for d10EB from *Dido3ΔCT* (blue bars), *Dido3ΔCT*+HA-DIDONT reconstituted (green bars) and *Dido3ΔCT*+HA-DIDONTΔNLS (red bars) determined by qRT-PCR. Data shown as mean ± SEM, $n = 3$.

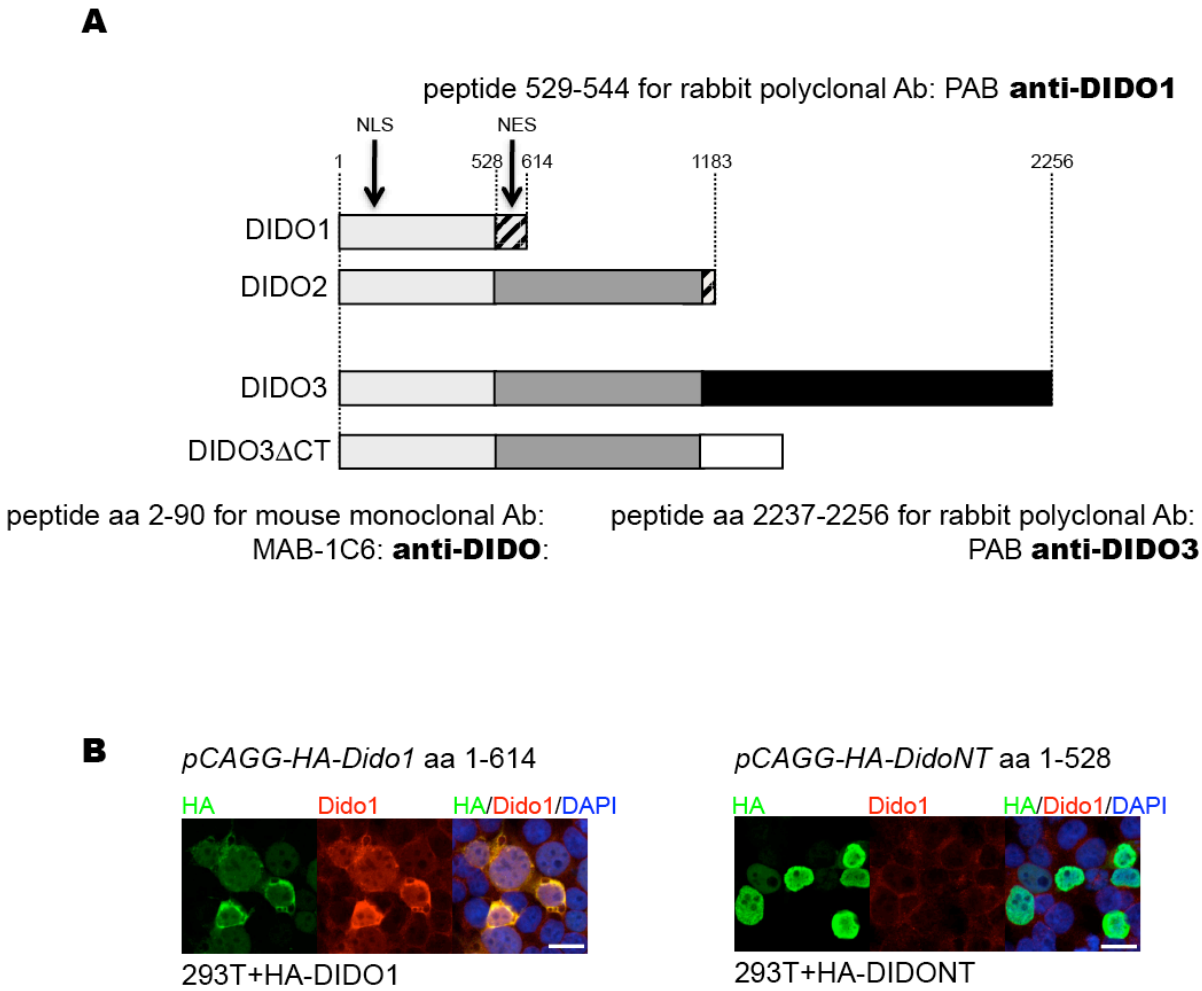

Figure S3. ***Details of different anti-DIDO isoform antibodies.*** **Related to Figure 2.** (**A**) Generation of anti-DIDO MAB-1C6 using the DIDO common N-terminal peptide, originally termed anti-CAS (common amino-terminal segment) (Prieto et al., 2009), of the polyclonal PAB-DIDO1 and PAB-DIDO3, each using isoform-specific C-terminal peptides; PAB-DIDO3 was previously described (Trachana et al., 2007). (**B**) Control staining for PAB-DIDO1 (red). Left, 293T cells expressing HA-DIDO1 with overlapping staining for PAB-DIDO1 (red) and anti-HA (green). Right, 293T cells expressing HA-DIDONT positive only for anti-HA (green). Nuclear counterstaining with DAPI (blue). Scale bars, 20 μm.

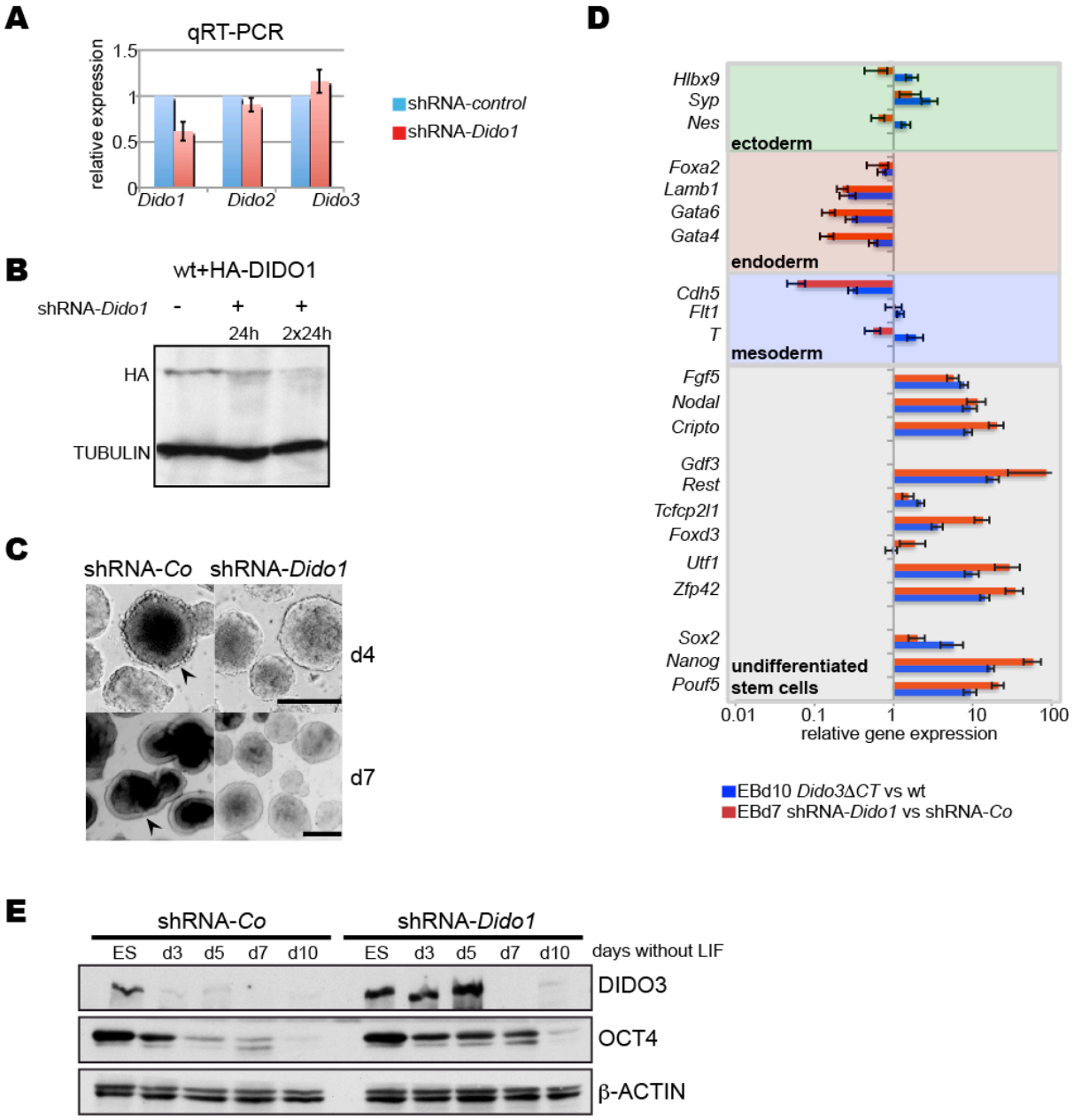

Figure S4. ***Additional controls for impaired differentiation capacity of shRNA-Dido1 ESC.*** **Related to Figure 3.** (**A**) Relative expression of *Dido* isoforms 1, 2 and 3, comparing shRNA-*control* cells (expression 1) and shRNA-*Dido1* cells determined by qRT-PCR. Data show mean ± SEM, $n = 3$. (**B**) shRNA-*Dido1* specificity confirmed in a western blot of wt cells with ectopic HA-DIDO1 expression; western blot developed with anti-TUBULIN as loading control. (**C**) Light microscopy images of d4- (top) and d10EB (bottom) of shRNA-*control* (left) and shRNA-*Dido1* (right) EB. Arrows indicate primitive endoderm in d4EB and further differentiation signs in d7EB. Scale bars, 100 μm. (**D**) Quantitative RT-PCR was used to determine the relative expression of selected markers for undifferentiated ESC, as well as endoderm, mesoderm and ectoderm in differentiating EB. d10EB of *Dido3ΔCT* (blue bars) and d7EB of shRNA-*Dido1* EB (red bars) were compared to wt or shRNA-*control* EB (baseline), respectively. Data show mean ± SEM, $n = 3$. (**E**) Expression of DIDO3 (top) and OCT4 (center) in lysates of ESC and of a d3-10EB time course in shRNA-*control* (left) vs shRNA-*Dido1* cells (right); β-ACTIN was used as loading control (bottom).

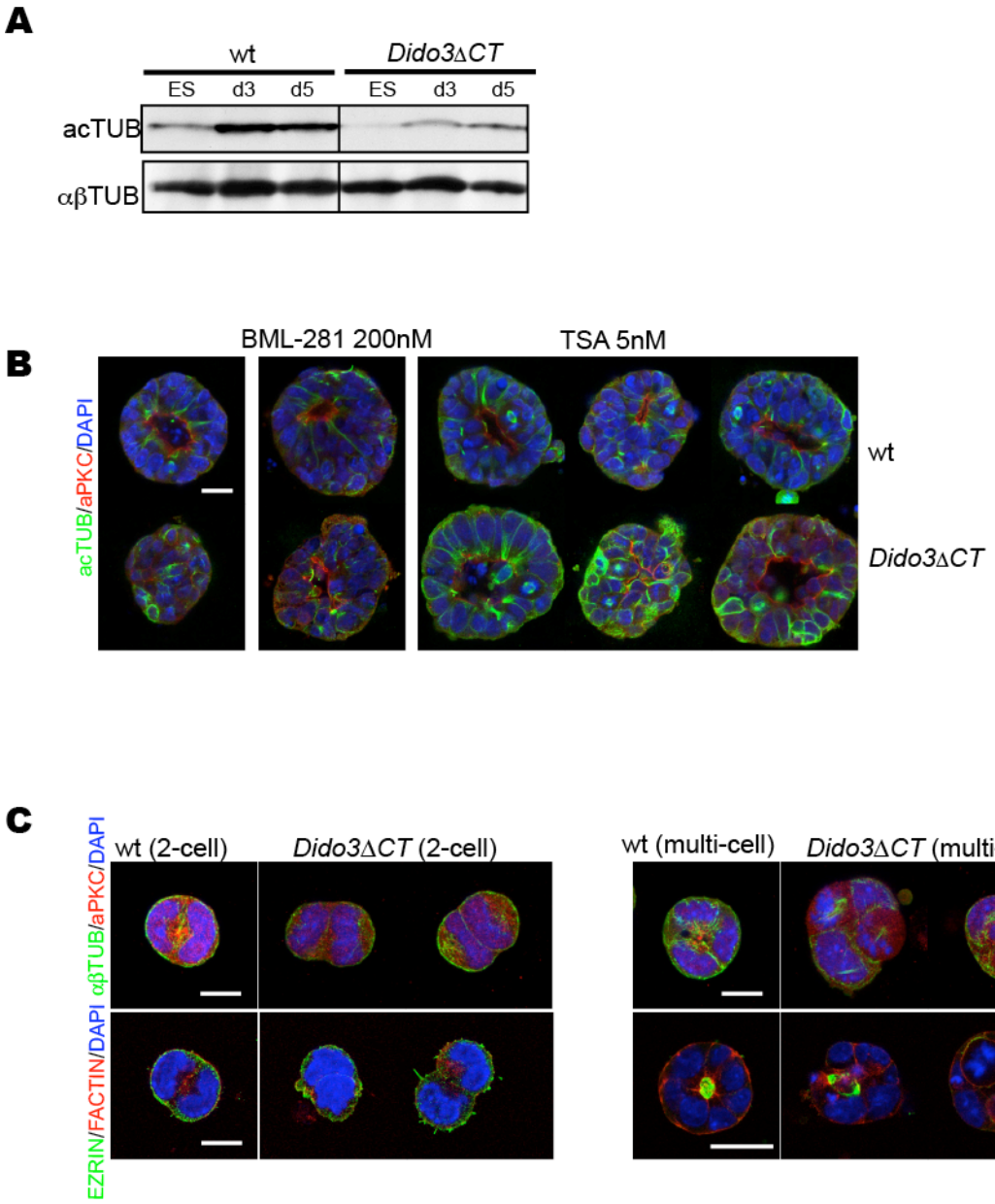

Figure S5. ***TUBULIN acetylation and organization in EB and rosettes.*** **Related to Figure 4.** (**A**) Western blot analysis of wt *vs Dido3ΔCT* lysates of ESC, d3EB and d5EB developed with anti-acetylated TUBULIN (top) or total -αβ-TUBULIN (bottom). (**B**) Treatment of rosettes with two HDAC inhibitors (untreated (left), BML-281-treated (center), or trichostatin (TSA)-treated (right)), rosettes of wt ESC (top) or *Dido3ΔCT* ESC (bottom) were stained with anti-acetylated TUBULIN (green) and -aPKC (red). (**C**) Comparison of wt vs *Dido3ΔCT*. Top, TUBULIN organization (green) and aPKC localization (red) in two-cell (left) and multi-cell rosettes (right); bottom, lumen formation marker EZRIN (green) and phalloidin label of F-ACTIN (red) of two-cell (left) and multi-cell (right) rosettes. (B,C) Nuclear counterstaining with DAPI (blue). Scale bars for 2-cell rosettes, 10 μm, multi-cell rosettes, 20 μm.

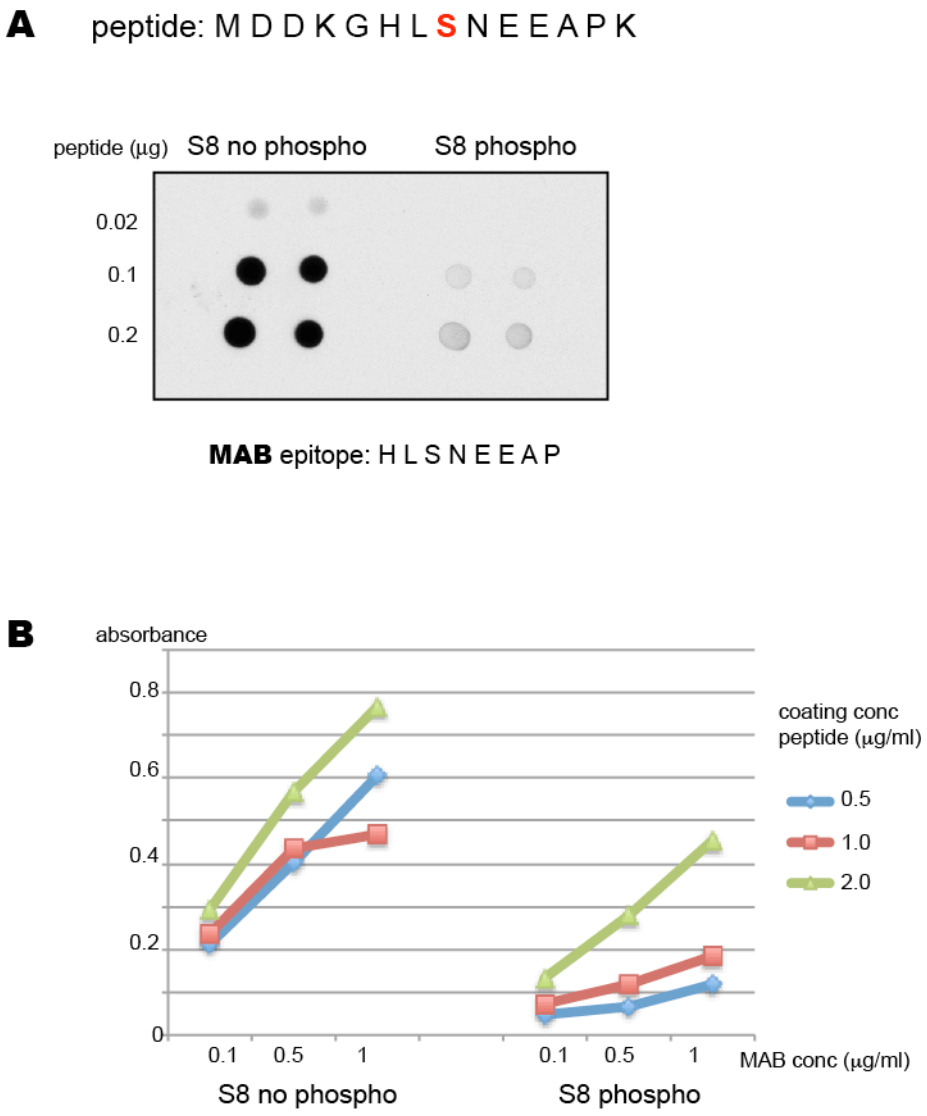

Figure S6. ***Epitope characterization of anti-DIDO MAB-1C6.*** **Related to Figure 5.** (**A**) Dot-blot analysis with MAB-1C6 for binding affinity to its epitope, which is dependent on phosphorylation on S8. We used the unphosphorylated (left) and S8-phosphorylated (right) peptides; both were dotted on nitrocellulose at three concentrations and developed with MAB-1C6 as for a standard western blot. (**B**) Standard ELISA procedure was used to test binding affinity of MAB-1C6 to both peptides (unphosphorylated *vs* S8-phosphorylated); different concentration combinations of antibody and coating peptides were tested.

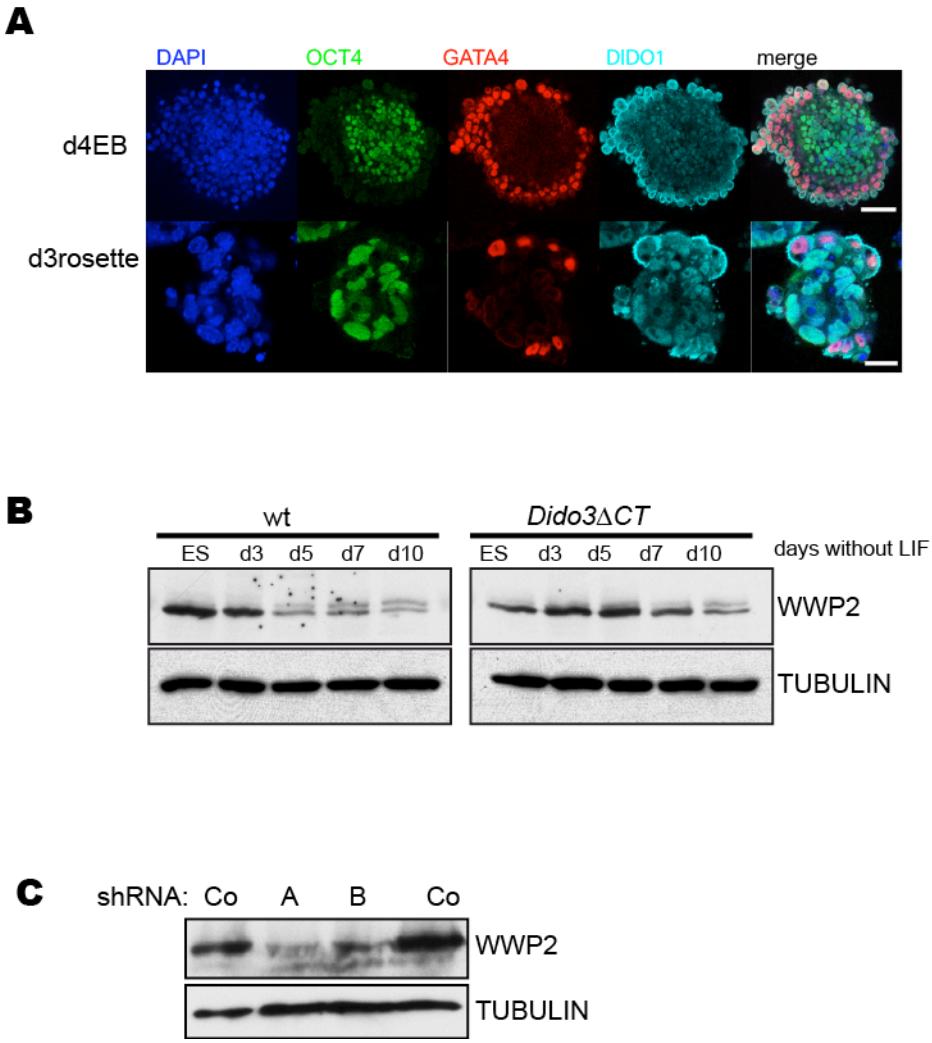

Figure S7. ***Cell fate markers of primitive endoderm (PE) and shRNA-Wwp2 controls.*** **Related to Figure 6.** (**A**) Characteristic staining pattern for PE cells in d4EB (top) and d3rosettes (bottom) with anti-OCT4 (green, negative in PE cells, positive inside EB), anti-GATA4 (red, positive only in PE cells), anti-DIDO1 (cyan, positive at apical membrane of PE cells and weak nuclear staining); nuclear counterstaining with DAPI (blue). Scale bars for EB, 50 μm; rosettes, 20 μm. (**B**) WWP2 expression in lysates of ESC and of a d3-10EB time course. Western blot analysis of wt (left) vs *Dido3ΔCT* (right) with anti-WWP2 (top) and -TUBULIN (bottom; loading control). (**C**) Top, WWP2 expression in shRNA-*control vs* two clones of shRNA-*Wwp2* A and B ESC. Bottom, loading control with anti-TUBULIN.

Table S1. ***Differentially expressed genes in EBd10 of Dido3ΔCT, Dido3ΔCT expressing HA-DIDO3CT or HA-DIDONT, all vs wt EBd10 with p <0.05, FDR <0.2 and fold change >2.*** **Related to Figure 1.**
RNA from three biological replicates was analyzed in Agilent microarrays. Data were normalized and filtered as described in Supplemental Experimental Procedures (below). Only statistically significant differentially expressed genes are shown.

Table S2. ***Gene lists used for GO analysis of differentially expressed probes in EBd10 of Dido3ΔCT, Dido3ΔCT reconstituted with HA-DIDO3CT or HA-DIDONT, all vs wt EBd10 2.*** **Related to Figure 1.** List of probes used for gene ontology enrichment analysis from Agilent microarrays of EBd10 (see Supp Table S2). Only GO biological process terms are described. Gene lists were created from HCL (hierarchical clustering) of statistically filtered data (see Supplemental experimental Procedures below).

Table S3, ***Differentially expressed genes of Dido3ΔCT ESC vs wt ESC with p <0.05, FDR <0.2 and fold change >2.*** **Related to Figure 2.** RNA from three biological replicates was analyzed in Affymetrix microarrays. Data were normalized and filtered as mentioned in Supplemental Experimental Procedures (below). Only statistically significant differentially expressed genes are shown.

Table S4. ***List of significant genomic intervals of ChIP-seq for HA-DIDO3 in ESC.*** **Related to Figure 7.**
Significant peaks were called by MACS v1.4 software, comparing experimental sample vs input. Eight peaks were identified for the *Dido* gene (in bold).

Supplemental Experimental Procedures

Microarrays

Affymetrix microarrays

RNA target preparation

Mouse embryonic stem cell cultures were harvested, snap-frozen in liquid nitrogen, and stored at -80°C. Total RNA was extracted using the guanidinium isothiocynate method (TRIzol reagent; Invitrogen, Carlsbad, CA), followed by purification using an RNeasy column (Qiagen, Valencia, CA). Each RNA preparation was tested for degradation using the Agilent 2100 Bioanalyzer (Agilent Technologies, Palo Alto, CA). cDNA was synthesized from 4 μg total RNA using One-Cycle target labeling and control reagents (Affymetrix, Santa Clara, CA) to produce biotin-labeled cRNA. The cRNA preparations (10 μg) were fragmented (94ºC, 35 min) into 35-200 bases in length.

Affymetrix microarray processing

GeneChip Mouse Genome 430 2.0 Array processing (hybridization, washing and scanning). Fragmented cRNA (10 μg) was hybridized to the mouse MOE 430 2.0 array (Affymetrix) containing 39000 transcript variants from 34000 well-characterized mouse genes. Each sample was added to hybridization solution containing 100 mM 2-(N-morpholino)ethanesulfonic acid, 1 M Na^+, and 20 mM EDTA, with 0.01% Tween-20 to a final cRNA concentration of 0.05 μg/ml. Hybridization was performed for 16 h at 45ºC. Each microarray was washed and stained with streptavidin-phycoerythrin in a Fluidics station 450 (Affymetrix) and scanned at 1.56 μm resolution in a GeneChip Scanner 3000 7G System (Affymetrix). Images were acquired and analyzed using GeneChip Operating Software (GCOS). Microarray processing, hybridization and initial statistical analysis were performed by the Genomics Facility at the Centro Nacional de Biotecnología.

Agilent microarray

RNA target preparation

Mouse embryoid bodies were harvested at day 10, snap-frozen in liquid nitrogen, and stored at -80°C. Total RNA was extracted using the guanidinium isothiocynate method (TRIzol reagent; Invitrogen), followed by purification using an RNeasy column (Qiagen). RNA quality was assessed using the Agilent Model 2100 Bioanalyzer (Agilent Technologies). For microarray use, 10 μg of total RNA was processed.

Agilent microarray processing

Agilent Mouse GE 4x44K v2 V2 (G4852A-028005). Array processing (hybridization, washing and scanning)
This microarray array is comprised of >44000 probe sets that interrogate 39430 transcripts and variants of the mouse genome. Probes were prepared and hybridization performed as described in the Two-Color Microarray Based Gene Expression Analysis Manual V. 6.5 (Agilent Technologies). Briefly, for each hybridization, 300 ng Cy3 probes and 300 ng Cy5 probes were mixed and added to 5 μl 10x Blocking Agent, 1 μl 25x Fragmentation Buffer and nuclease-free water in a 25 μl reaction, incubated (60ºC, 30 min) to fragment RNA, and the reaction terminated with 25 μl 2x Hybridization Buffer. Samples were placed on ice, quickly loaded onto arrays, hybridized in a hybridization oven rotator (65ºC, 17 h), then washed in GE Wash Buffer 1 (room temperature, 1 min) and in GE Wash Buffer 2 (37ºC, 1 min). Arrays were dried by centrifugation (2000 rpm, 2 min). Images were captured with an Agilent Microarray Scanner and spots quantified using Feature Extraction Software (Agilent Technologies). Microarray processing, hybridization and initial statistical analysis were performed by the Genomics Facility at the Centro Nacional de Biotecnología.

Sequences

For shRNA-*Dido1*, GIPZ lentiviral particles with the *Dido1*-specific target sequence CTCTCTGGGTGGTTCCTAA (Thermo Scientific).

For shRNA-*Wwp2*, retroviral vector pGFP-V-RS with four different 29mer shRNAs to murine *Wwp2* target sequences (Origene):
GTCAACCTCTCCAATGTCCTGAAGAACAA; GCACTTCAGCCAAAGATTCCTCTACCAGT; GTTCTGGCAGGTTGTCAAGGAGATGGACA; AAGGCTCACCTGGTGCCTATGACCGAAGT

For Q-PCR, *Dido* proximal promotor FW primer CGGAATCCGGTGCTGGTTTG; RV primer CATTTCCAGAGCTACCACGG; *Dido* intern side FW primer CTACACCTGGTTATCCACTGC; RV primer GCAGAGACCAACTCTTGCAAG

Peptide scan for epitope determination of MAB-1C6. Peptide scanning procedure to identify the epitope recognized by anti-DIDO MAB-1C6. A set of dodecapeptides consecutively shifted by two amino acids along the target sequence were synthesized automatically and linked directly to an activated membrane in a spot array. The target was the predicted amino acid sequence of mouse DIDO protein between positions 2-95. The membrane was blocked and analyzed by standard western blot, with digital imaging of chemiluminescent signal. MAB-1C6 specifically illuminated three spots that shared the HLSNEEAP sequence (residues 6-13 of murine DIDO protein).

Antibodies used in these experiments

Specificity	Antibody	Dilution	Source, reference	Technique
DIDO1	Rabbit polyclonal	1:400	Our laboratory, PAB-Dido1	IF
DIDO3	Rabbit polyclonal	1:400	Our laboratory, PAB-Dido3	IF
NT-DIDO	Mouse monoclonal	1:100	Our laboratory, Dido MAB-1C6	IF, WB
OCT4	Mouse monoclonal	1:100 1:1000	Santa Cruz, sc-5279	IF WB
GATA4	Goat polyclonal	1:200	R&D Systems	IF
HA-tag	Mouse monoclonal	1:500 1:1000	Covance, MMS-101P	IF WB
HA-tag	Rabbit polyclonal	1:1000 3-5 μg	Abcam; ChIP grade ab9110	IF, WB IP
FOCA2	Goat polyclonal	1:100	R&D Systems; af2400	IF
MEGALIN	Goat polyclonal	1:100	Santa Cruz; sc-16478	IF
aPKC	Rabbit polyclonal	1:200 1:2000	Santa Cruz; sc-216	IF WB
γ-TUBULIN	Mouse monoclonal	1:1000	Sigma-Aldrich; T6557	IF
γ-TUBULIN	Rabbit polyclonal	1:1000	Sigma-Aldrich; T3320	IF
acetylated-TUBULIN	Mouse monoclonal	1:400 1:2000	Sigma-Aldrich; T7451	IF WB
αβ-TUBULIN	Mouse monoclonal	1:500	Abcam; ab44928)	IF
WWP2	Rabbit polyclonal	1:200 5 μg	Bethyl; A302-936A	IF IP
WWP2	Goat polyclonal	1:200	Santa Cruz; sc-11896	WB
β-ACTIN	Mouse monoclonal	1:3000	Sigma-Aldrich; A3853	WB
EZRIN	Rabbit polyclonal	1:200	Cell Signalling; 3145	IF
RNAPOL II	Rabbit polyclonal	1:1000 1 μg	Santa Cruz; sc-899	WB IP
F-ACTIN	Phalloidin	1:500	Invitrogen; A 12381	IF
Nucleus	DAPI counterstain	1:300	Invitrogen; D 1306	

IF, immunofluorescence; WB, Western blot; IP, immunoprecipitation

Phosphopeptide analysis by LC-MS/MS ion trap

Phosphopeptide purification. The enrichment procedure concatenates two in-house-packed microcolumns, the immobilized metal affinity chromatography (IMAC) microcolumn and the Oligo R3 reverse-phase column, which provide selective purification and sample cleanup, respectively, prior to LC-MS/MS analysis. LC-MS/MS was performed as reported (Navajas et al., 2011).

Analysis by LC-MS/MS ion trap, alternating CID/ETD fragmentation techniques (collision-induced dissociation, CID;, electron transfer dissociation, ETD). Reverse-phase liquid chromatography was performed on an Ultimate 3000 nanoHPLC (Dionex, Amsterdam, The Netherlands). A 5 μl volume of reconstituted peptide sample was injected on a C18 PepMap trap column (5 μm, 100 Å, 300 μm ID x 5 mm) at a 30 μl/min flow rate, using H_2O:AcN:TFA (98:2:0.1) as loading mobile phase (5 min). The trap column was then switched on-line in back-flush mode to a C18 PepMap 100 analytical column (3 μm, 100 Å, 75 μm ID x 15 cm).

The micropump provided a 300 nl/min flow-rate and was operated in gradient elution conditions, using 0.1% formic acid in water as mobile phase A, and 0.1% formic acid in 80% acetonitrile/20% water as mobile phase B. Gradient elution conditions were as follows: isocratic conditions of 4% B (5 min), a linear increase to 50% B (in 60 min), a linear increase to 95% B (2 min), isocratic conditions of 95% B (4 min), and return to initial conditions in 2 min. The column was re-equilibrated for 15 min. Wavelengths were monitored at 214 and 280 nm with a UV detector.

NanoHPLC was coupled to a 3D ion trap mass spectrometer Amazon speed (Bruker Daltonics, Bremen, Germany) via CaptiveSpray ion source operating in positive ion mode, with capillary voltage set at 1.3 kV. The ion trap mass spectrometer was operated in a data-dependent mode, performing full scan (m/z 350-1500) MS spectra followed by tandem MS, alternating CID/ETD fragmentation of the eight most abundant ions. Dynamic exclusion was applied to prevent the same m/z from being isolated for 0.2 min after its fragmentation. For peptide identification, CID and ETD spectra were validated manually.

Chromatin-IP sequencing. DNA amount was determined by Picogreen and fragment size in a Bioanalyzer; fragments were within expected size distribution (125-325 bp). Libraries were generated from 5-10 ng DNA with Trueseq DNA Sample Preparation kit (Illumina) following the manufacturer's protocol, with modifications: no in-line control, Ampure purification step was replaced by purification with MinElute

(Qiagen); adaptor ligation with 1/100 adaptor dilution, PCR for enrichment of DNA fragments with 15 cycles. For high-throughput sequencing we used Illumina Sequencing Technology on an Illumina Genome Analyzer II (all steps performed by the Genomic Service Unit, Parque Científico de Madrid).

Bioinformatics analysis

Statistical analysis of Affymetrix microarray data

For analyses, we used the affylmGUI R package (Wettenhall *et al*., 2006). The robust multiarray analysis (RMA) algorithm was used for background correction, normalization and expression level summarization (Irizarry *et al*., 2003). This was followed by differential expression analysis with Bayes t-statistics from the linear models for microarray data (Limma) included in the affylmGUI package (Smyth, 2004; Smyth and Speed, 2003). P-values were corrected for multiple testing using the Benjamini-Hochberg method (Benjamini and Hochberg, 1995) and false discovery rate (Reiner *et al*., 2003). Genes were considered to be differentially expressed if the FDR was <0.2 (all selected probes with p-values <0.05). In addition, only probes with a fold-change variation >2 were considered for further analysis.

Statistical analysis of Agilent microarray data

Analysis was performed using the Limma and the non-parametric algorithm 'Rank Products' packages available at Bioconductor (Huber *et al*., 2015). P-values were corrected for multiple testing using the Benjamini-Hochberg method and FDR. Genes were considered differentially expressed and selected for further study when the Limma FDR was <0.2 (all selected probes with adjusted p-values <0.05) and a 2-fold change difference was found in expression values.

Statistical analysis of ChIP-seq

DNA from immunoprecipitated chromatin was sequenced in a GAII Illumina sequencer. Sequences in FASTQ format were mapped to the mouse genome (NCBI Build 37/UCSC mm9) using BOWTIE aligner (bowtie2 v2.0.6; (Langmead and Salzberg, 2012). Resulting BAM files were transformed into SAM format with Samtools (v1.3.1. view, sort, index; (Li et al., 2009) and resulting SAM files were used to define binding regions. Peak calling software MACS (v1.4; (Zhang et al., 2008) was used to identify significant peaks by comparing experimental IP and input control data with default parameters (band width = 300, model fold = 10,30, p-value cutoff = 1.00e-05). A total of 2888 significant peaks were finally called.

Other ChIP-seq data

From (Brookes et al., 2012):
GEO accession data - GSE34520

-RNApolIInoP-GSM850469_RNAPII_8WG16.bw
-RNApolIIS5P-GSM850467_RNAPII_S5P.bw
-RNApolIIS2P-GSM850470_RNAPII_S2P.bw
-RNApolIIS7P-GSM850468_RNAPII_S7P.bw

Bing Ren, Ph.D. http://bioinformatics-renlab.ucsd.edu/rentrac/
and
An integrated encyclopedia of DNA elements in the human genome.
ENCODE Project Consortium. Nature. 2012 Sep 6;489(7414):57-74. doi: 10.1038/nature11247.

H3K4me3	https://www.encodeproject.org/files/ENCFF001KEH
H3K9ac	https://www.encodeproject.org/files/ENCFF001KDA
H3K27ac	https://www.encodeproject.org/files/ENCFF001KDN
H3K4me1	https://www.encodeproject.org/files/ENCFF001KEH
H3K36me3	https://www.encodeproject.org/files/ENCFF001KDY
H3K27me3	https://www.encodeproject.org/files/ENCFF001KDS
H3K9me3	https://www.encodeproject.org/files/ENCFF001KDG

Further post-processing analysis

FIESTA viewer (http://bioinfogp.cnb.csic.es/tools/FIESTA/index_server.php) was used for data visualization of microarray data (Oliveros, 2007). The Integrative Genomics Viewer (IGV, http://www.broadinstitute.org/igv) (Robinson et al., 2011) (Thorvaldsdottir et al., 2013) was used for visualization and exploration of genomic datasets. MeV (MultiExperiment Viewer (http://www.tm4.org/mev.html) (Saeed *et al*., 2003) was used for gene clustering of Agilent microarray data. For clustering, first a list of significant probes was obtained for any of the three conditions tested (2403 probes). Probes with no change (<1.5-fold change) in control vs Dido3ΔCT condition were removed. The resulting probe list (1531 probes) was passed to the MeV application and HCL clustering was performed (Eisen *et al*., 1998). Probes were then manually assigned to six distinct gene expression profile groups and individual probe lists for each group were analyzed for Gene Ontology biological process enrichments online in the DAVID website, using mouse annotations as background for comparison (DAVID Bioinformatics Resources 6.7, https://david.ncifcrf.gov/home.jsp; (Huang da et al., 2009a, b).

Supplemental References

Benjamini, Y., and Hochberg, Y. (1995). Controling the false discovery rate: a practical and powerful approach to multiple testing. J Roy Stat Soc B 57, 289-300.

Brookes, E., de Santiago, I., Hebenstreit, D., Morris, K.J., Carroll, T., Xie, S.Q., Stock, J.K., Heidemann, M., Eick, D., Nozaki, N., et al. (2012). Polycomb associates genome-wide with a specific RNA polymerase II variant, and regulates metabolic genes in ESCs. Cell Stem Cell 10, 157-170.

Eisen, M.B., Spellman, P.T., Brown, P.O., and Botstein, D. (1998). Cluster analysis and display of genome-wide expression patterns. Proc Natl Acad Sci USA 95, 14863-14868.

ENCODE Project Consortium. An integrated encyclopedia of DNA elements in the human genome. Nature. 2012 Sep 6;489(7414):57-74.

Huang da, W., Sherman, B.T., and Lempicki, R.A. (2009a). Bioinformatics enrichment tools: paths toward the comprehensive functional analysis of large gene lists. Nucleic Acids Res 37, 1-13.

Huang da, W., Sherman, B.T., and Lempicki, R.A. (2009b). Systematic and integrative analysis of large gene lists using DAVID bioinformatics resources. Nat Protoc 4, 44-57.

Huber, W., Carey, V.J., Gentleman, R., Anders, S., Carlson, M., Carvalho, B.S., Bravo, H.C., Davis, S., Gatto, L., Girke, T., et al. (2015). Orchestrating high-throughput genomic analysis with Bioconductor. Nat Methods 12, 115-121.

Irizarry, R.A., Hobbs, B., Collin, F., Beazer-Barclay, Y.D., Antonellis, K.J., Scherf, U., and Speed, T.P. (2003). Exploration, normalization, and summaries of high density oligonucleotide array probe level data. Biostatistics 4, 249-264.

Langmead, B., and Salzberg, S.L. (2012). Fast gapped-read alignment with Bowtie 2. Nat Methods 9, 357-359.

Li, H., Handsaker, B., Wysoker, A., Fennell, T., Ruan, J., Homer, N., Marth, G., Abecasis, G., Durbin, R., and Genome Project Data Processing, S. (2009). The Sequence Alignment/Map format and SAMtools. Bioinformatics 25, 2078-2079.

Navajas, R., Paradela, A., and Albar, J.P. (2011). Immobilized metal affinity chromatography/reversed-phase enrichment of phosphopeptides and analysis by CID/ETD tandem mass spectrometry. Methods Mol Biol 681, 337-348.

Oliveros, J.C. (2007). FIESTA@BioinfoGP. An interactive server for analyzing DNA microarray experiments with replicates (http://bioinfogp.cnb.csic.es/tools/FIESTA).

Reiner, A., Yekutieli, D., and Benjamini, Y. (2003). Identifying differentially expressed genes using false discovery rate controlling procedures. Bioinformatics 19, 368-375.

Robinson, J.T., Thorvaldsdottir, H., Winckler, W., Guttman, M., Lander, E.S., Getz, G., and Mesirov, J.P. (2011). Integrative genomics viewer. Nat Biotechnol 29, 24-26.

Saeed, A.I., Sharov, V., White, J., Li, J., Liang, W., Bhagabati, N., Braisted, J., Klapa, M., Currier, T., Thiagarajan, M., et al. (2003). TM4: a free, open-source system for microarray data management and analysis. Biotechniques 34, 374-378.

Smyth, G.K. (2004). Linear models and empirical bayes methods for assessing differential expression in microarray experiments. Stat Appl Genet Mol Biol 3, Article3.

Smyth, G.K., and Speed, T. (2003). Normalization of cDNA microarray data. Methods 31, 265-273.

Thorvaldsdottir, H., Robinson, J.T., and Mesirov, J.P. (2013). Integrative Genomics Viewer (IGV): high-performance genomics data visualization and exploration. Brief Bioinform 14, 178-192.

Trachana, V., van Wely, K.H., Guerrero, A.A., Futterer, A., and Martinez, A.C. (2007). Dido disruption leads to centrosome amplification and mitotic checkpoint defects compromising chromosome stability. Proc Natl Acad Sci USA 104, 2691-2696.

Wettenhall, J.M., Simpson, K.M., Satterley, K., and Smyth, G.K. (2006). affylmGUI: a graphical user interface for linear modeling of single channel microarray data. Bioinformatics 22, 897-899.

Zhang, Y., Liu, T., Meyer, C.A., Eeckhoute, J., Johnson, D.S., Bernstein, B.E., Nusbaum, C., Myers, R.M., Brown, M., Li, W., et al. (2008). Model-based analysis of ChIP-Seq (MACS). Genome Biol 9, R137.